Handbook of Conducting Polymers
Fourth Edition

CONJUGATED POLYMERS

Properties, Processing, and Applications

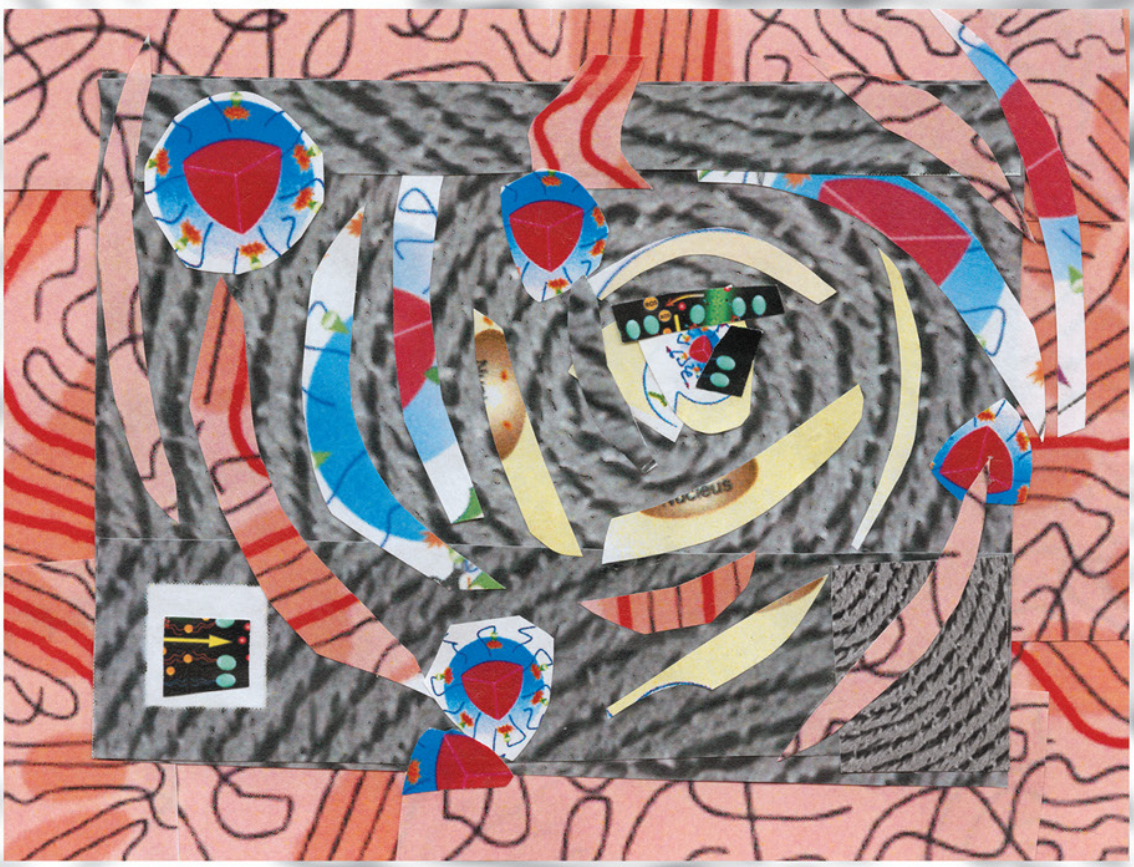

Edited by
John R. Reynolds, Barry C. Thompson, and Terje A. Skotheim

CRC Press
Taylor & Francis Group

7

Mechanical Properties of Semiconducting Polymers

Mohammad A. Alkhadra, Andrew T. Kleinschmidt, Samuel E. Root, Daniel Rodriquez, Adam D. Printz, Suchol Savagatrup, and Darren J. Lipomi

7.1 Introduction and Background

Semiconducting polymers have always been associated with flexible applications, such as solar cells, active-matrix displays, and biomedical sensors.[1,2] Mechanical flexibility of these materials, however, is not automatic. The mechanical properties of semiconducting polymers must be engineered by tuning the chemical structure, molecular weight, processing conditions, and interactions with other materials in the device stack.[3,4] Despite the importance of mechanical deformability in essentially all applications of semiconducting polymers, mechanical properties have, until recently, been an afterthought. For example, the mechanical stability of organic solar cells has often been overlooked in favor of improving

power conversion efficiencies. However, the development of semiconducting polymers that can endure the rigors of roll-to-roll coating, survive long term against mechanical deformations in the outdoor environment, and withstand packing and transportation in portable devices demands an understanding of their mechanical properties. These properties—including elasticity, extensibility, strength, and toughness—are critically dependent not only on the molecular structure of the materials but on the ways these structures pack in the solid state, which are, in turn, mediated by the conditions of processing. Prediction of the mechanical behavior of materials in a device is confounded by the fact that the properties of materials measured in the laboratory can depend on testing conditions, such as temperature, strain rate, and choice of substrate.

The mechanical properties of polymers, at the most basic level, can be usefully classified according to their response to applied loads (glassy or rubbery) and the corresponding mechanism of fracture (brittle or ductile). The mechanical response and fracture mechanism of any polymer under deformation can be captured in a stress–strain curve, an idealized example of which is shown in Figure 7.1. For a given material, a stress–strain curve reveals mechanical properties such as the elastic modulus, yield point, and toughness. The mechanical property to be optimized depends on the application. For example, bonding a device to a nonplanar surface such as a lens or windshield may require large extensibility that need not be reversible (i.e., plastic as opposed to elastic), while incorporating such a material into a device to be worn on the skin, which is reversibly deformable, requires the opposite. Applications that will be subject to twisting and shear deformations require high cohesive and adhesive energies within and between the layers in the device stack. The mechanisms by which semiconducting polymers store or dissipate mechanical energy depend on many of the same characteristics that influence the mechanical behavior of commodity polymers and engineering plastics: e.g., the barriers to molecular rotation, degree of crystallinity, glass transition temperature. The ways in which semiconducting polymers mediate mechanical energy also depend, however, on characteristics that are rarely found in conventional polymers: e.g., stiffness of the π-conjugated backbone, the flattened, anisotropic shape of a polymer chain, and the ubiquitous presence of side chains.

7.1.1 Semiconducting Polymers as a Subset of All Solid Polymers

The presence of solubilizing pendant groups in semiconducting polymers is required for solution processing, as the unsubstituted main chain of a π-conjugated polymer is generally insoluble.[4] Semiconducting polymers are rendered soluble by the attachment of alkyl side chains, which afford solubility by weakening strong van der Waals interactions between main chains and by conferring greater entropic freedom of the polymer in solution.[5] These side chains also strongly affect the thermomechanical properties and

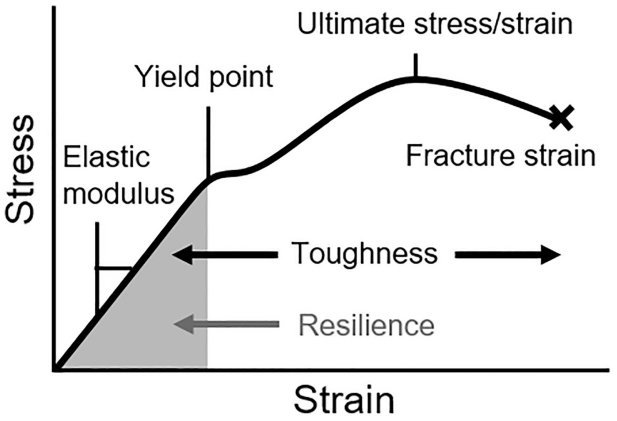

FIGURE 7.1 A hypothetical stress–strain curve illustrating its most important features.

solid-state packing. Among these "comb-like" polymers, the side chains in the solid state can point end-to-end or they can interdigitate. A polymer whose side chains interdigitate is often stiffer and more brittle because of increased crystallinity. Improved molecular packing in crystalline regions also results in an anisotropic elastic modulus due to unequal densities of van der Waals interactions in orthogonal directions (e.g., π–π stacking vs interactions between interdigitated side chains).

Analysis of the mechanical properties of commodity polymers and engineering plastics is a well-established discipline. Semiconducting polymers, however, differ from conventional, non-conjugated plastics in a number of ways. These differences include obvious dissimilarities in chemical structure—namely, increased stiffness of the backbone due to π-conjugation—and practical considerations such as the availability of materials for mechanical testing. Conventional pull-testing of a solid polymer to obtain a stress–strain curve often requires large quantities of the material. Pilot-scale syntheses of semiconducting polymers, however, typically produce materials in quantities sufficient to fabricate only thin films (~100 nm).[4] While the thin film is the only geometry of these materials used in devices, it is inconvenient to measure the mechanical response of a thin film. Methods have thus been developed specifically to determine the mechanical properties of thin films of semiconducting polymers, though the choice of method often has an effect on the mechanical response. Conveniently, the mechanical properties of semiconducting polymers are intrinsically coupled to their thermal properties and phase transitions, and these transitions—in particular, the glass transition temperature, assuming it too can be measured—may be used to predict at least some of the mechanical behavior.

The thermal transition of semiconducting polymers which perhaps most greatly influences the mechanical response is the glass transition, and the temperature at which it occurs (T_g). Traversing the T_g corresponds to a second-order phase transition from a glass to a rubbery solid. The transition is also characterized by an increase in heat capacity, specific volume, and deformability.[6–8] While the T_g of conventional plastics is usually determined calorimetrically, the small change in heat capacity of semiconducting polymers around the T_g is often difficult to detect, though several methods have been developed to circumvent this difficulty.[7,9]

Experimental methods developed to understand the thermomechanical properties of semiconducting polymers—especially the aspects of semiconducting polymers that differ from conventional polymers—have been supplemented by computation.[8,10] When semiconducting polymers are processed from solution, the morphology that forms upon evaporation of the solvent is often difficult to predict. Theoretical models have thus been developed to investigate the nanoscale structural characteristics and conformational behavior that control the mechanical properties of semiconducting polymers and—as are required for organic solar cells—their composites with soluble fullerenes.[11]

Effects of molecular mixing on the thermomechanical behavior of polymer–fullerene composites, such as stiffening and embrittling of the polymer, are the result of molecular recognition (i.e., intercalation of fullerenes between side chains) and corresponding changes in microstructural order. Indeed, the solid-state packing structure, as it is determined by molecular structure and solid-state microstructure, greatly influences the mechanical properties of semiconducting polymers.[12] The following sections discuss the elementary principles that govern the mechanical properties of semiconducting polymers and the ways in which these materials mediate mechanical energy.

7.2 Deformation in Solid Polymers

Depending on the type of material, geometry of the specimen, and conditions of the applied forces, different modes of deformation may occur on the application of tension, compression, shear, or twisting. As these different forces are applied to an object, intermolecular forces arise in the deformed body to resist or minimize deformation. On the application of sufficiently large loads, however, the deformed body may break to dissipate mechanical energy. Deformation may also occur as a result of changes in temperature; in this case, thermal energy induces change in the shape and size of an object (e.g., expansion or contraction).

7.2.1 Mediation of Mechanical Energy

The mechanical response of a solid polymer is governed principally by two structures which are characterized by different length scales: the molecular structure (~1 Å – 10 nm) and the solid-state microstructure (~10 nm – 100 nm). The molecular structure controls the mechanical response by bonding topology, molecular weight, and other parameters at the scale of individual chains. The microstructure determines the mechanical response based on the degree of crystallinity, the glassy state, and the allowance of slip in the crystalline domains. The evolution in the structure of a solid polymer at various size scales upon deformation—i.e., from the bending, stretching, and breaking of covalent bonds to the deformation of entire crystallites—serves to either store or dissipate mechanical energy. The ways in which a solid polymer stores or dissipates this energy can be classified by its modes of deformation: elastic deformation, plastic deformation, and fracture.

At small strains, glassy polymers, in which little molecular motion is allowed, exhibit linear elastic behavior that is driven by an enthalpic response to mechanical deformation, as polymer chains are displaced from local minima in potential energy. Further elongation of glassy samples causes non-reversible deformations due to sliding and alignment of chains in response to tensile stress. These deformations may occur at constant volume (i.e., shear yielding) or they may be dilatational (i.e., crazing) depending on the degree of entanglement of chains. On the other hand, in rubbery polymers (elastomers), in which considerable molecular motion is allowed, the polymer chains behave as entropic springs: upon elongation, a reduction in the number of conformations available to chains decreases the entropy of the system. This decrease in entropy generates a restoring force that causes chains to relax to their equilibrium states upon releasing the applied strain.

When the applied strain is sufficiently large, solid polymers fracture by either cohesive failure—which occurs when the cohesive energy of the material is overcome—or adhesive failure—which occurs as a result of debonding at the interface between a polymer and the underlying substrate. These modes of deformation in any solid polymer—from linear elasticity to fracture—are all, in turn, affected by the thermomechanical properties of the material and thus the phase of the solid polymer.

7.2.2 Elasticity and Plasticity

For semicrystalline polymers below T_g, elasticity is mediated by van der Waals forces and deformation of covalent bonds. On experimentally relevant time scales, relaxation of polymer chains in such materials is prohibited, which reduces the rotational and translational mobility that these chains can exhibit. Conversely, for semicrystalline polymers above the glass transition temperature, chains are allowed to reorganize and align along the axis of applied tensile strain due to a reduction in viscosity. The resulting decrease in internal, or entropic, degrees of freedom upon deformation and concomitant restoring force is the basis of linear elasticity in solid polymers. This elastic behavior terminates either with brittle fracture or with plastic deformation followed by ductile fracture.

The yield point marks the onset of plastic deformation, at which point the mechanical energy stored during elastic behavior is dissipated plastically. In other words, polymers chains adopt new configurations at mechanical equilibrium once the elastic strain energy exceeds intermolecular and entropic forces in the elastic regime. This plastic deformation is generally non-reversible and occurs due to sliding and alignment of chains in response to tensile stress. Such mobility of polymer chains is facilitated by a low T_g but may be hindered due to the existence of strong intermolecular forces uniformly in a polymer crystal. For example, interdigitation between side chains in the crystalline domains of semicrystalline semiconducting polymers causes these materials to exhibit brittle behavior, instead of plastic deformation, to dissipate mechanical energy.

7.2.3 Fracture

The total energy per unit volume that a material can absorb before fracture is known as its toughness. Cyclic or intermittent loading can lower the elasticity and toughness by the accumulation of chain

scission and microstructural rearrangement produced by strain and local heating. For samples with low molecular weight and therefore low densities of entanglements, pullout of polymer chains can become a dominant mechanism of fracture. Fracture in a real sample is also triggered by the presence of defects in solid films. That is, mechanical energy is concentrated in the vicinity of small inhomogeneities, such that fracture occurs due to the enlargement of these regions.[13] Under tensile elongation, the mechanism of fracture may be determined by the shape of the stress–strain curve (Figure 7.1). Moreover, the nature of the fracture surface differs considerably[14] between cracked thin films of brittle and ductile polymers. In contrast to brittle solids, plasticity contributes to the fracture of ductile solids. A plastic zone develops at the tips of cracks in ductile materials, and energy is dissipated primarily due to plastic flow in the material near these crack tips, rather than due to the creation of new surfaces. In either brittle or ductile materials, fracture produces a new surface, the formation of which is balanced by the dissipation of elastically stored energy.

The cohesion of a semiconducting polymer determines in large part its mechanical reliability and resistance to fracture, necessary for deformable applications. The criterion that best portends the fracture of a solid material or interface is the strain-energy release rate, G (in J m^{-2}), which is defined as the energy available for unit increase in crack length, $2c$:

$$G = \frac{dW}{dA} - \frac{dU}{dA} = \frac{1}{h}\left(\frac{dW}{dc} - \frac{dU}{dc}\right) \tag{7.1}$$

where W is the external work being done on the system, U is the elastically stored energy, A is the surface area of the crack, and h is the thickness of the specimen. It is assumed that fracture occurs when G exceeds the critical value G_c, known as the cohesive fracture energy.[13] This energy is the combined energy of various dissipative processes, which include molecular deformations, plastic flow in fracture process zones (i.e., regions of damage around crack tips), and scission of chemical bonds. The cohesive energy, which may be determined using double cantilever beam or four-point bending tests,[4] depends on van der Waals interactions, chemical bonding, and the degree of entanglement.

An entanglement is defined as a physical linkage between two polymer chains whereby molecules can slide past but not through each other. Greater degrees of entanglement correspond to larger values of the cohesive energy. The density of entanglements in a polymer scales with its molecular weight and directly controls the mechanisms of energy dissipation in the fracture process zone. Increasing the molecular weight of a semiconducting polymer results in more extensive plastic deformation and frictional pullout of chains prior to cohesive failure. Eventually, sufficient entanglement entails scission of chemical bonds upon fracture. The cohesion thus strongly influences the mechanical properties and mechanisms of fracture.[15]

7.3 Mechanical Properties and Measurement Techniques

It is generally challenging to measure the mechanical properties of thin films for two reasons. First, handling these films for a conventional pull test is difficult. Second, pilot-scale syntheses typically do not produce material in quantities large enough for testing more than a few films. These challenges have been met by the development of different methods that facilitate the handling of thin films to determine their mechanical response to tensile strain.

7.3.1 Overview of Mechanical Properties

The classical way to obtain the mechanical response of a material is through a stress–strain curve (Figure 7.1). The slope of the linear region gives the elastic modulus of a material. This parameter is a measure of the capacity of a material to reversibly store mechanical energy—and thus its resistance to elastic deformation. The area under the linear region is the resilience, which is the maximum energy density that a

material can store before exhibiting irreversible plastic deformation. The yield stress corresponds to the stress at which the material deforms plastically and permanently (i.e., when the mechanical response becomes driven by sliding and alignment of chains). Graphically, the yield stress is represented by the point past which the stress–strain curve becomes nonlinear. The highest point reached on the vertical axis of a stress–strain curve corresponds to the ultimate stress (or strength) and ultimate strain. The strain (stress) at which the material ruptures is known as the fracture strain (stress). Finally, the area under the entire curve is the toughness, which is the maximum energy density that a material can absorb before mechanical failure.

7.3.2 Common Measurement Techniques

There are three common approaches for measuring the mechanical properties of thin films of semiconducting polymers. The first approach (Figure 7.2a) is referred to as the film-on-water technique: a thin film is supported on the surface of water and subjected to a uniaxial pull test. A stress–strain curve is then produced by measuring the force required to elongate the film by a set distance. The second approach (Figure 7.2b) is a suite of methods referred to as film-on-elastomer techniques. To approximate the mechanical response of semiconducting polymers to tensile strain, the film-on-elastomer method consists of three separate experiments in which a thin film is supported by an elastomer such as poly(dimethylsiloxane) (PDMS). The third approach (Figure 7.2c and Figure 7.2d) is to determine the adhesion and cohesion of thin films by measuring applied forces (e.g., due to bending) versus displacement of a beam or cantilever. Other techniques to quantify the mechanical properties of semiconducting polymers and their blends with fullerenes have been developed. These techniques involve either atomic force spectroscopy,[16] nanoindentation,[17] or scratch testing.

The film-on-water method is a pseudo freestanding tensile test.[18,21] This method leverages the high surface tension and low viscosity of water to provide an almost frictionless support for thin films. The film-on-water method works well for a range of semiconducting polymers so long as the materials do not interact with water, particularly through dissolution or swelling. Soft, elastomeric grips are used to make contact between the fragile thin films, linear actuator, and force-sensing equipment. One of the primary advantages of the film-on-water method is that it allows the acquisition of a complete trace of force as a function of displacement that, along with the dimensions of the sample, can be used to generate a stress–strain curve. The mechanical properties of solid polymers, however, depend on the rate of applied strain: higher strain rates generally lead to greater elastic moduli when testing viscoelastic materials such as semiconducting polymers. A more complete description of the effects of strain rate on the mechanical properties of polymers is given in Section 7.4.3.

The film-on-elastomer method consists of a buckling-based metrology,[22] laser determination of the yield point (LADYP),[19] and crack-onset strain measurement.[23] The buckling technique, shown schematically in Figure 7.2b (top), is used to determine the elastic modulus of thin films of semiconducting polymers based on well-established buckling mechanics.[24] Mechanical buckling occurs when a relatively stiff and thin film is compressed on a compliant, thick substrate. This compression produces a buckling instability due to the balance between the energy required to deform the soft substrate and the energy required to bend the stiff film. This instability manifests as a sinusoidal wrinkling pattern with a well-defined wavelength. At some critical wavelength, which is a function of the material properties of both the film and the substrate, the total strain energy in the system is minimized. The buckling wavelength, λ_b, may be used to calculate the elastic modulus of the film, E_f, using the relation

$$E_f = 3E_s\left(\frac{1-\nu_f^2}{1-\nu_s^2}\right)\left(\frac{\lambda_b}{2\pi h}\right)^3 \tag{7.2}$$

where E_s is the elastic modulus of the substrate, h is the film thickness, and ν_f and ν_s are the Poisson ratios of the film and the substrate, respectively.

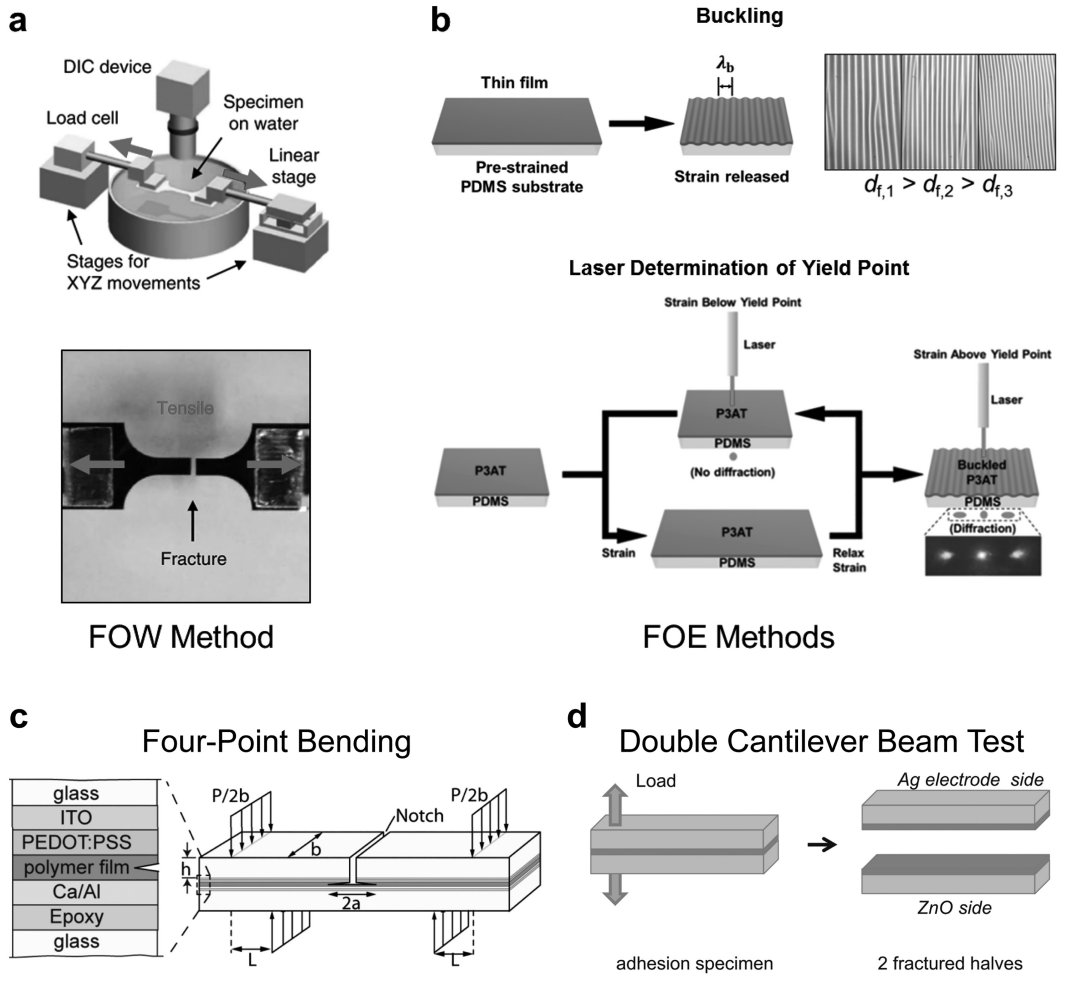

FIGURE 7.2 Common methods used to determine the mechanical properties of thin films of semiconducting polymers. (a) Diagram of the film-on-water testing procedure; the system for tensile testing consists of a linear stage, a load cell, and a digital image correlation (DIC) camera. Reproduced with permission from Kim et al., *Nat. Commun.* 2013, 4, 2520. Copyright 2013, Nature Publishing Group. (b) Diagrams of the film-on-elastomer testing procedures, namely buckling and laser determination of the yield point (LADYP). Reproduced with permission from Printz et al. *ACS Appl. Mater. Interfaces* 2015, 7, 23257–23264. Copyright 2015, American Chemical Society. (c) Schematic of the experimental setup for four-point bending in which the specimen has a starter notch that is equidistant from the pins on the side under tension; *P* is the applied force. Reproduced with permission from Balar et al., *Macromolecules* 2017, 50, 8611–8618. Copyright 2017, American Chemical Society. (d) Schematic of the experimental setup for the double cantilever beam test by which a pristine specimen is separated into two fractured halves. Reproduced with permission from Dupont et al., *Org. Electron.* 2013, 14, 1262–1270. Copyright 2013, Elsevier.

LADYP, shown in Figure 7.2b (bottom), is a film-on-elastomer technique used to determine the yield point of thin films by identifying the termination of their elastic behavior.[19] To implement the LADYP test, thin films are transferred to an elastomeric substrate and are subjected to cyclic, incremental strain in steps of 1%—i.e., 0% → 1% → 0% → 2% → 0% → 3% → 0%, and so forth. Periodic wrinkles are formed when the yield point, or onset of plastic deformation, of the material is reached. These wrinkles can be visualized either directly using an optical microscope or indirectly through their manifestation of a diffraction pattern when irradiated with a laser beam.

Measurement of crack-onset strain is the simplest film-on-elastomer technique and is used to estimate the strain at fracture of a thin film supported by an elastomer.[25] For this test, a polymer film is transferred to an elastomeric substrate, uniaxially strained in increments of 1%, and imaged under an optical microscope. The crack-onset strain is then identified as the strain at which cracks or pinholes first appear in the film. This measurement, however, is limited by the resolution of the microscope. Moreover, cracking behavior in supported films is dependent on both adhesion and the mismatch between the elastic moduli of the film and the substrate: a greater elastic mismatch produces lower crack-onset strains (increased effective brittleness).[26–29]

Adhesion and cohesion are two mechanical properties that accurately quantify and describe the fracture behavior of a thin film. Films that poorly adhere to the substrate are susceptible to delamination, and films that poorly cohere are likely to crack or bifurcate. Adhesion and cohesion are functions of van der Waals interactions, chemical bonding, and the density of entanglements.[4] Common techniques to determine the adhesion and cohesion of a thin film include four-point bending and the double cantilever beam test. Four-point bending is best suited to measure interfacial adhesion between layers, though it may also be used to measure the cohesion of individual layers. This technique involves loading a film between two beams and applying a force using bending pins, as shown in Figure 7.2c. The sandwiched film has a starter notch that is equidistant from the pins on the side under tension. To direct the propagation of this notch to the interface of interest, a small area of material known to have poor adhesion is often incorporated. The experimental setup for the double cantilever beam test consists of a single film or multiple films placed between two beams. As shown in Figure 7.2d, a force is applied normal to the surface at one end of each beam. Similar to four-point bending, the double cantilever beam test can be used to quantify both adhesive and cohesive fracture of thin films.

7.4 Effects of Physical Parameters

The mechanical properties of thin films of semiconducting polymers are influenced by a wide range of experimentally controllable parameters that are distinct from molecular structure. These physical parameters include substrate compliance, film thickness—which is directly affected by processing conditions—and strain rate. Changes in these parameters primarily manifest as increases or decreases in the strain-energy release rate upon elongation.[27,28] The thickness of the film may also influence the measured cohesive energy, as the size of the plastic zone may be geometrically confined by the boundaries of the specimen to a smaller volume.[14] In addition, fracture processes are dominated by viscoelastic relaxation mechanisms, which correspond to a dependence on the strain rate. It follows that the mechanical properties of thin films of semiconducting polymers (as in a device) can be modulated by parameters other than the chemical structures of these materials.

7.4.1 Effects of Elastic Mismatch and Adhesion

The strain-energy release rate (Equation (7.1)) is a function of the mismatch between the elastic moduli of the film and the substrate.[27] This dependence is a consequence of stress localization at the interface of a strained bilayer structure, such as a rigid film supported by a compliant substrate, with increasing elastic mismatch. The elastic mismatch may be quantified using Dundurs' parameters α and β:[26,27]

$$\alpha = \frac{\bar{E}_f - \bar{E}_s}{\bar{E}_f + \bar{E}_s}, \beta = \frac{1}{2}\frac{\mu_f(1-2\nu_s) - \mu_s(1-2\nu_f)}{\mu_f(1-\nu_s) + \mu_s(1-\nu_f)} \tag{7.3}$$

where $\bar{E} = E/(1-\nu^2)$, ν is the Poisson ratio, $\mu = E/(2(1+\nu))$, and subscripts 'f' and 's' denote the film and the substrate, respectively. For stiff films of semiconducting polymers and relatively compliant substrates of PDMS, $E_f \gg E_s$ implies that $\alpha \approx 1$. Furthermore, the dependence of G on β is weak when $\alpha > 0$

and β may be neglected, but *G* becomes an increasingly strong function of α as α tends to 1; in particular, *G* increases with increasing α.[27,28] Since α quantifies the mismatch between the elastic moduli of the film and the substrate, *G* exceeds G_c (Section 7.2.3) at comparatively lower strains for systems with greater elastic mismatch. Consequently, the more compliant the substrate, the lower the strain at fracture of the supported polymer film, and vice-versa.[29] This effect of elastic mismatch is shown microscopically in Figure 7.3a, where samples of 40 kDa poly(3-hexylthiophene) (P3HT) exhibit greater crack densities at 20% applied strain when supported by more compliant PDMS substrates.[30] Adhesion between the film and the substrate is also an important consideration regarding substrate effects on the mechanical properties of thin films. For plastically deformable films of metal supported by polymeric foils, an adhesion layer suppresses the formation and propagation of microcracks.[31] Moreover, semiconducting polymer films exhibit a significant increase in extensibility upon encapsulation, which is the result of forced Poisson compression and stress delocalization over the films by the encapsulating substrate.[32]

7.4.2 Effects of Film Thickness

Thickness affects virtually all aspects of thin-film behavior, especially for thicknesses below 100 nm (Figure 7.3b and Figure 7.3c). The dependence of thermomechanical behavior on film thickness is complex. The contribution of a plastic zone that dissipates elastic strain energy at crack tips[14] is appreciable in materials of high molecular weight (Figure 7.3b), which exhibit a significant density of entanglements.[15,33] The volume of this plastic zone may be geometrically confined by elastic boundary layers (e.g., adjacent layers in a device stack) as the film is made thinner. A small plastic zone, however, does

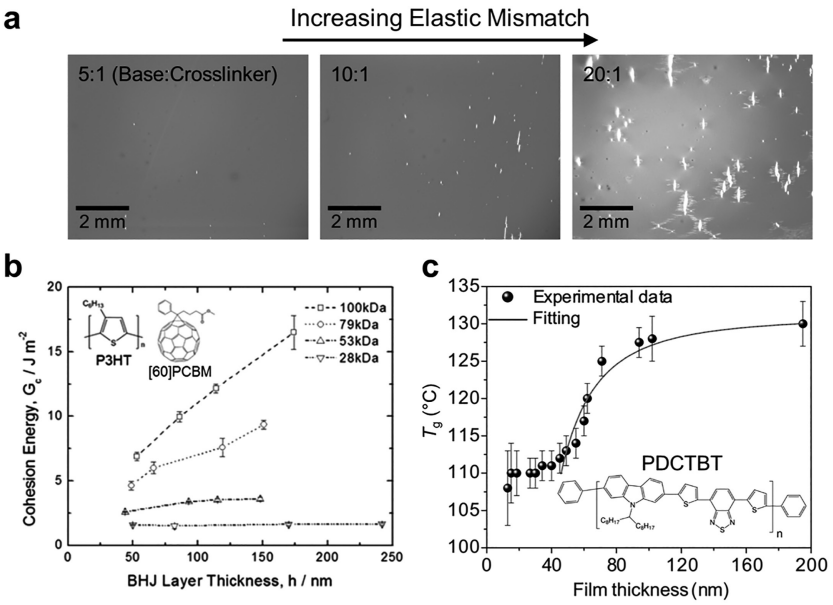

FIGURE 7.3 Physical parameters affecting the measurement of mechanical properties. (a) Optical micrographs showing samples of 40 kDa P3HT with varying crack densities on PDMS at 20% applied strain; the larger the PDMS curing ratio (base:crosslinker), the more compliant the PDMS, and thus the greater the elastic mismatch. Reproduced with permission from Rodriquez et al., ACS *Appl. Mater. Interfaces* 2017, 9, 8855–8862. Copyright 2017, American Chemical Society. (b) Dependence of the cohesive energy, G_c, of a bulk-heterojunction layer (regioregular P3HT:[60]PCBM) on film thickness, h, and P3HT molecular weight. Reproduced with permission from Bruner et al., *Macromolecules* 2014, 47, 1117–1121. Copyright 2014, American Chemical Society. (c) Glass transition temperature, T_g, of PCDTBT as a function of film thickness; the regression[34] is based on a phenomenological two-layer model. Reproduced with permission from Wang et al., *Eur. Phys. J. E. Soft Matter* 2012, 35, 9807. Copyright 2012, Springer.

little to dissipate mechanical stress through plastic flow, and thus the material ruptures more readily in thinner films than for thicker films, at least for polymers of high molecular weight.[15,33] The cohesive energy of polymers of high molecular weight is therefore strongly dependent on thickness, as shown in Figure 7.3b, due to significant plastic flow at the tips of cracks that initiate in pre-existing defects.[33] Indeed, thicker films of a particular semiconducting polymer of high molecular weight exhibit greater ductility compared to thinner ones.[14,15] Specifically, there is a marked decrease in the tendency for cracks to propagate in thicker films during tensile loading.

For ultrathin (<100 nm) films, however, the appearance of cracks may be suppressed for a different reason: namely increased mobility of polymer chains and reduced density of entanglements due to skin-depth effects. The contribution of a mechanically soft, loosely entangled network of chains, which exists near the surface of polymer films, becomes more prominent as the film is thinned below 100 nm.[36–38] This free surface in a geometrically confined polymer film depresses the T_g due to the enhanced dynamics and segmental mobility of polymer chains (see Figure 7.3c for the case of PCDTBT).[35] The loosely entangled network of chains in turn lowers the elastic modulus of the film, reduces its fracture strength, and increases (albeit slightly) its strain at fracture.[39] These skin-depth effects can occur in any polymer film, brittle or ductile, regardless of whether or not a plastic zone exists. Two conclusions can thus be drawn: first, a reduction in intermolecular entanglement density near the free surface of a thinned film enhances segmental mobility and weakens intermolecular forces, both of which soften the material. Second, highly mobile chains at the free surface can effectively relieve mechanical stress induced during elongation.

7.4.3 Effects of Strain Rate

In stress–strain measurements of polymers, higher strain rates generally result in greater apparent elastic moduli.[30] Consistent with previous work on non-conjugated polymers,[40,41] films of 63 kDa P3HT were tested at two strain rates, and the greater strain rate produced a larger apparent elastic modulus (Figure 7.4). An increasing strain rate relative to the timescales of chain reptation results in an effective stiffening of the material and thus an increase in its elastic modulus.[41]

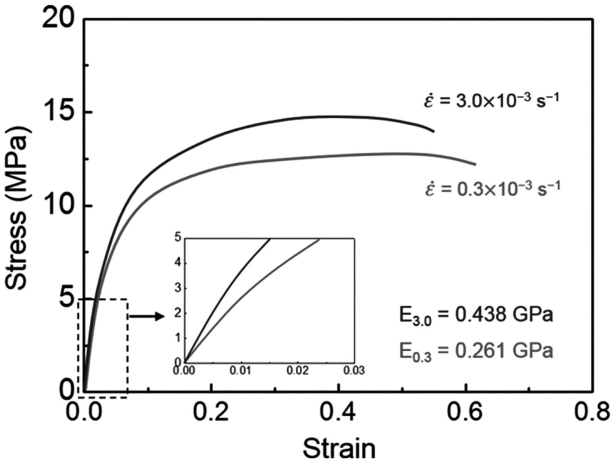

FIGURE 7.4 Effects of strain rate on the mechanical properties of semiconducting polymers. Stress–strain curves of thin films of 63 kDa P3HT obtained by film-on-water tensile testing at two different strain rates; the pull test performed at the greater strain rate resulted in a larger apparent elastic modulus. Reproduced with permission from Rodriquez et al., *ACS Appl. Mater. Interfaces* 2017, 9, 8855–8862. Copyright 2017, American Chemical Society.

7.5 Effects of Molecular Structure and Microstructure

The molecular weight, length of solubilizing alkyl side chains, and chemical structure of the backbone all influence the plasticity of thin films of semiconducting polymers. The mechanical properties of these materials are also affected by the morphology and packing structure in the solid state, which can be influenced strongly by processing conditions and the kinetics of solidification of films cast from solution.

7.5.1 Role of Molecular Weight

The degree of polymerization of a polymer is quantified by its molecular weight, the distribution of which is reported as either a weight-average, M_w, or a number-average, M_n, molecular weight. Typically, M_w is a more realistic predictor of the mechanical properties of polymers because it is weighted toward the degrees of polymerization that make up the largest weight fraction of the sample. Molecular weight has a large influence on the cohesion and plasticity of thin films of semiconducting polymers.[30,42] For example, the cohesive energy of P3HT:[60]PCBM bulk heterojunction solar cells increases with increasing molecular weight of P3HT (Figure 7.3b) due to plastic dissipation of elastic strain energy.[33] Higher molecular weights can also increase the extensibility of poly(3-alkylthiophene)s (P3ATs), which has been measured in the form of a bulk tape (Figure 7.5a)[42] and as a thin film (Figure 7.5b and Figure 7.5c).[30] The increase in plasticity and cohesion of the films with molecular weight is due to an increase in the

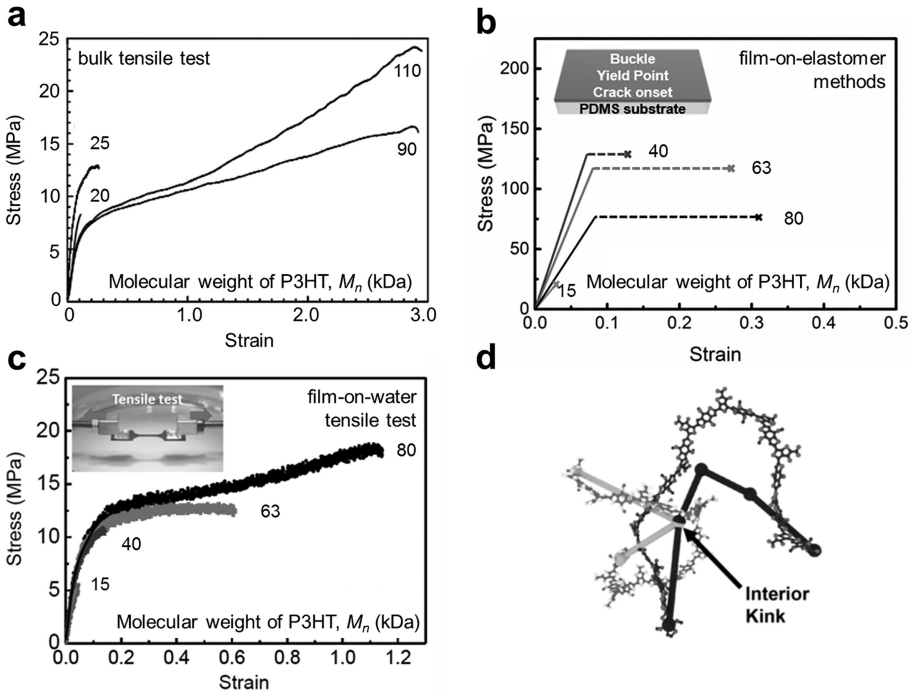

FIGURE 7.5 Role of molecular weight on the mechanical properties of P3HT. (a) Bulk tensile testing of P3HT tapes with different molecular weights that were solidified from a melt phase. Reproduced with permission from Koch et al., *Prog. Polym. Sci.* 2013, 38, 1978–1989. Copyright 2013, Elsevier. (b) Film-on-elastomer methods and (c) film-on-water tensile testing of thin films of P3HT with different molecular weights. Reproduced with permission from Rodriquez et al., *ACS Appl. Mater. Interfaces* 2017, 9, 8855–8862. Copyright 2017, American Chemical Society. (d) Representation of an interior kink that results in an entanglement between two polymer chains. Reproduced with permission from Root et al., *Energy Environ. Sci.* 2016, 10, 558–569. Copyright 2017, Royal Society of Chemistry.

density of entanglements. The density of entanglements is proportional to the number of interior kinks (Figure 7.5d) in the chains, which increases with degree of polymerization.[43,44] In a theoretical framework, an interior kink occurs at the intersection of the primitive paths of entangled polymer chains. Entanglements raise the energy needed for frictional pullout.[33] In general, semiconducting polymers above a critical molecular weight ($M_c \approx 10$ kDa for P3HT in principle[45]) will exhibit greater viscosity, ultimate strength, toughness, and extensibility due to the entanglement of chains compared to the same material below its M_c.[42]

7.5.2 Role of Alkyl Side Chains

The unsubstituted π-conjugated main chain of semiconducting polymers is not readily soluble. To render these materials soluble, alkyl side chains are typically attached. Side chains confer solubility by interrupting van der Waals interactions between main chains and by permitting greater entropic freedom of the polymer in solution. These side chains also influence the thermomechanical properties. In P3ATs, longer alkyl side chains increase the crack-onset strain and lower the elastic modulus (Figure 7.6).[46,47] In fact, the steepest decrease in modulus with increasing side-chain length, n, coincides with the point at which the T_g drops well below room temperature (~25°C), which occurs between $n = 6$ and $n = 7$ for P3ATs.[46,48] (The T_g of P3HT appears to be a borderline case and has been reported to span a range of temperatures, from approximately –16°C to 35°C.[7]) Since the side chains of P3ATs typically do not interdigitate in the solid state,[12,49] increased length of side chains results in weaker van der Waals interactions between polymer chains.[48] This reduction in intermolecular bond strength allows for greater disorder in the system and ability to dissipate mechanical stress. In a similar manner, branched side chains promote microstructural disorder due to steric hindrance and increased free volume between neighboring main chains,[50] which decreases the crystalline correlation lengths of both π–π stacking and lamellar spacing.[51]

7.5.3 Role of Molecular Structure and Backbone Rigidity

Molecular ordering in semiconducting polymers, particularly intermolecular ordering induced by interdigitation of side chains and crystallization, results in increased elastic moduli and decreased strains at fracture.[49,52] The rigidity of the backbone can affect the mechanical properties of semiconducting polymers;[25] specifically, inflexible backbones may be expected to reduce the flexibility of thin films.

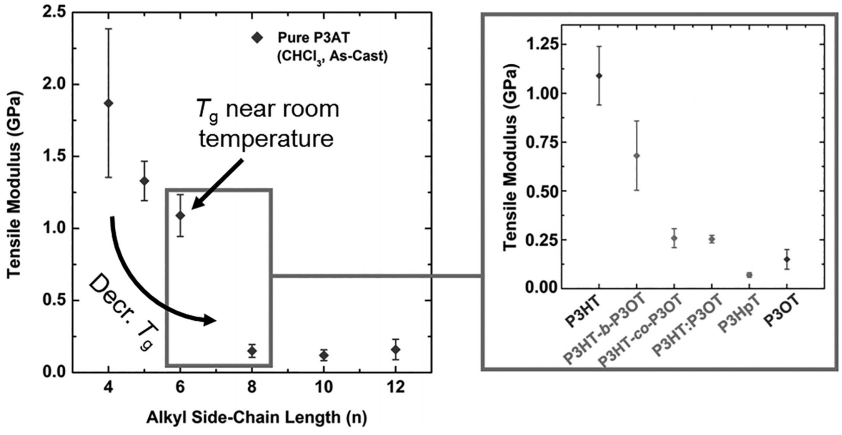

FIGURE 7.6 Role of the length of alkyl side chains on the tensile modulus of P3ATs. The greatest deviation in modulus occurs when the length of alkyl side chains is increased from $n = 6$ to $n = 7$, which is most likely due to the depression of T_g below room temperature for $n = 6$. Reproduced with permission from Savagatrup et al., *Macromolecules* 2014, 47, 1981–1992. Copyright 2014, American Chemical Society.

Indeed, a correlation between rigid backbones and stiffer films is often observed when incorporating fused rings.[25,53] In contrast, polymer chains can be made more flexible by adding aliphatic spacers to the backbone, which disrupt conjugation and allow for greater exploration of conformational space. Changes in molecular properties by modification of the backbone, however, can altogether change the packing structure. Effects of backbone rigidity are thus often partially or entirely overwhelmed by competing effects of microstructural packing (Figure 7.7).[53–55] Because of this interplay of effects, the greatest role that backbone rigidity plays on the mechanical properties of semiconducting polymers is through modulation of the T_g.[7] This role is especially prominent when the glass transition occurs below room temperature.

7.5.4 Role of Intermolecular Packing

Interdigitation of side chains, and the resulting inhibition of molecular motion, can embrittle semiconducting polymers.[12,25,56] The consequences of interdigitation are seen most clearly in the case of P3HT, the side chains of which can interdigitate upon solvent annealing (called "form II").[49,57] The interdigitated form of P3HT is more brittle than the non-interdigitated form ("form I").[49] Branched side chains generally inhibit interdigitation, and non-interdigitated microstructures exhibit decreased elastic modulus and increased crack-onset strain.[25] The effect of order in a film, especially as a result of increased regioregularity (as in P3ATs), is generally to stiffen and embrittle.[52]

7.6 Glass Transition Temperature and Measurement Techniques

The viscosity of a solid polymer controls the time scales that are required for reorganization of chains in the amorphous domains. These time scales decrease exponentially with increasing temperature, particularly as the sample passes through the glass transition, characterized by T_g (generally a small range of temperatures), for which several measurement techniques exist.

7.6.1 The Glass Transition in Semiconducting Polymers

As temperature is increased, polymers can reversibly pass to a progressively more fluid and rubbery state, which results in changes in density, viscosity, and refractive index. These changes occur due to

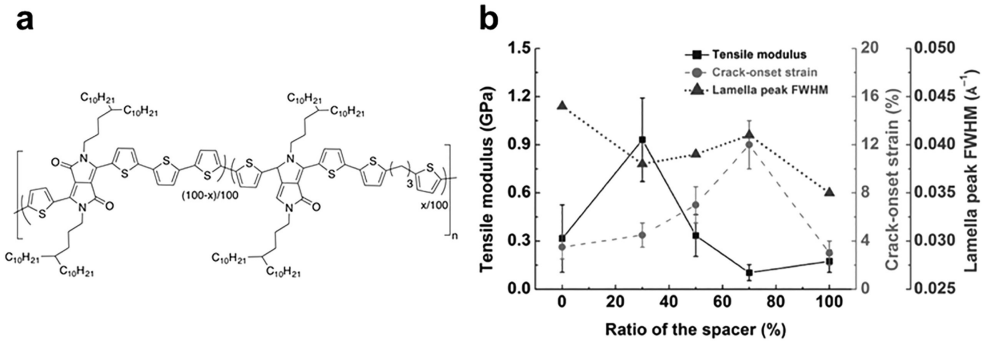

FIGURE 7.7 Conjugation-break spacer (CBS) in a DPP-based polymer and the impact on the mechanical properties of thin films. (a) Chemical structure of the DPP-*x* polymers bearing a CBS in varying proportions; *x* represents the percentage of the CBS added, with $x = 0$ corresponding to full rigidity and $x = 100$ corresponding to full flexibility along the backbone. (b) Mechanical properties and microstructural data of the DPP-*x* polymers; measurements of tensile moduli and crack-onset strains show no clear trends with increasing percentage of the CBS, as changes in packing structure overshadow decreased backbone rigidity. Reproduced with permission from Savagatrup et al., *Macromol. Rapid Commun.* 2016, 27, 1623–1628. Copyright 2016, Wiley-VCH Verlag, GmbH & Co. KGaA.

relaxation of the main chain (thermally activated translational and rotational modes of motion).[7,58] The nominal temperature that marks the onset of this second-order, non-isothermal phase transition is defined as T_g. At operating temperatures well below the T_g, segmental relaxation is prohibited on experimental time scales, such that existing chain conformations are frozen in metastable states.[7,59] The mechanical degradation of thin films (e.g., during tensile deformation) can be mitigated by decreasing the T_g,[60,61] which is achieved by increasing the length of side chains (see Section 7.5.2).[47] In Figure 7.8, strains of 10% were applied to films of poly(3-hexylthiophene) and poly(3-dodecylthiophene) (P3DDT) blended with [6,6]-phenyl C_{61} butyric acid methyl ester ([60]PCBM). Upon visual inspection, major cracks on the surface of the P3HT:[60]PCBM film, though not on the surface of the P3DDT:[60]PCBM film, can be observed.[47] Increased ductility in the latter film is due to a reduced T_g and thus improved resistance to decohesion through viscoelastic dissipation of mechanical energy.[46,62]

At operating temperatures well above the T_g, segmental relaxation processes and the associated rate of intermolecular rearrangement can occur on experimentally relevant time scales that decrease exponentially with increasing temperature according to the Vogel–Fulcher law.[58] The resulting decrease in viscosity above the T_g allows polymer chains to reorganize and chain segments to relax towards thermodynamic equilibrium.[59,63] Above the T_g, thin films of semiconducting polymers can exhibit plastic deformation, which aids in accommodating mechanical stresses and dissipating elastic strain energy.[7,62] Furthermore, temperature-dependent phenomena in polymeric materials, such as viscoelastic stress relaxation, phase separation, and crystallization, occur more readily above the T_g.

7.6.2 Techniques to Measure the T_g of Semiconducting Polymers

The T_g is a critical property of materials that is difficult to determine for thin films of semiconducting polymers, despite its importance in predicting the thermal and mechanical stabilities of these materials. There are several techniques to measure the T_g of semiconducting polymers, including differential scanning calorimetry (DSC),[64] dynamic mechanical analysis (DMA),[65] variable-temperature ellipsometry (VTE),[66] and ultraviolet–visible (UV–vis) spectroscopy.[9] DSC is performed by heating (or cooling) a sample along with an inert reference and measuring the difference in heat flow (Figure 7.9a, left). This difference, typically recorded as a function of temperature (Figure 7.9a, right), arises due to the release or absorption of heat during phase transitions such as crystallization (release) or melting (absorption).[7] As shown in Figure 7.9a, the glass transition corresponds to a change in heat capacity of the sample,[67] i.e., a change in the slope of its DSC thermogram. The sensitivity of a DSC measurement could be amplified by increasing the scan rate, for instance to detect indistinct signals of weak thermal transitions. Conventional DSC setups, however, are limited to bulk samples and cannot be used to study thin films and their thermal properties, which exhibit a non-trivial dependence on thickness below a critical threshold (Figure 7.3c) due to geometric confinement and interfacial effects.[35,68]

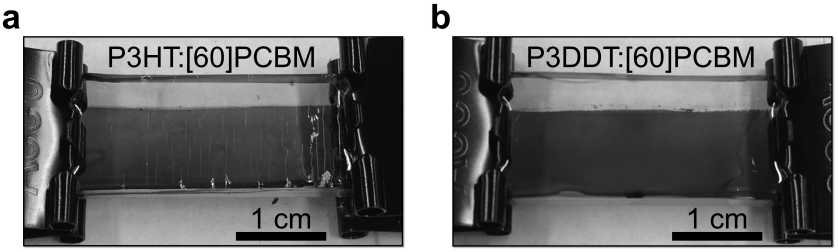

FIGURE 7.8 Variation in the mechanical response of films of polymer–fullerene composites with T_g. Optical micrographs of thin films of (a) P3HT:[60]PCBM and (b) P3DDT:[60]PCBM on PDMS under an applied strain of 10%. Reproduced with permission from Savagatrup et al., *Adv. Funct. Mater.* 2014, 24, 1169–1181. Copyright 2014, Wiley-VCH Verlag, GmbH & Co. KGaA.

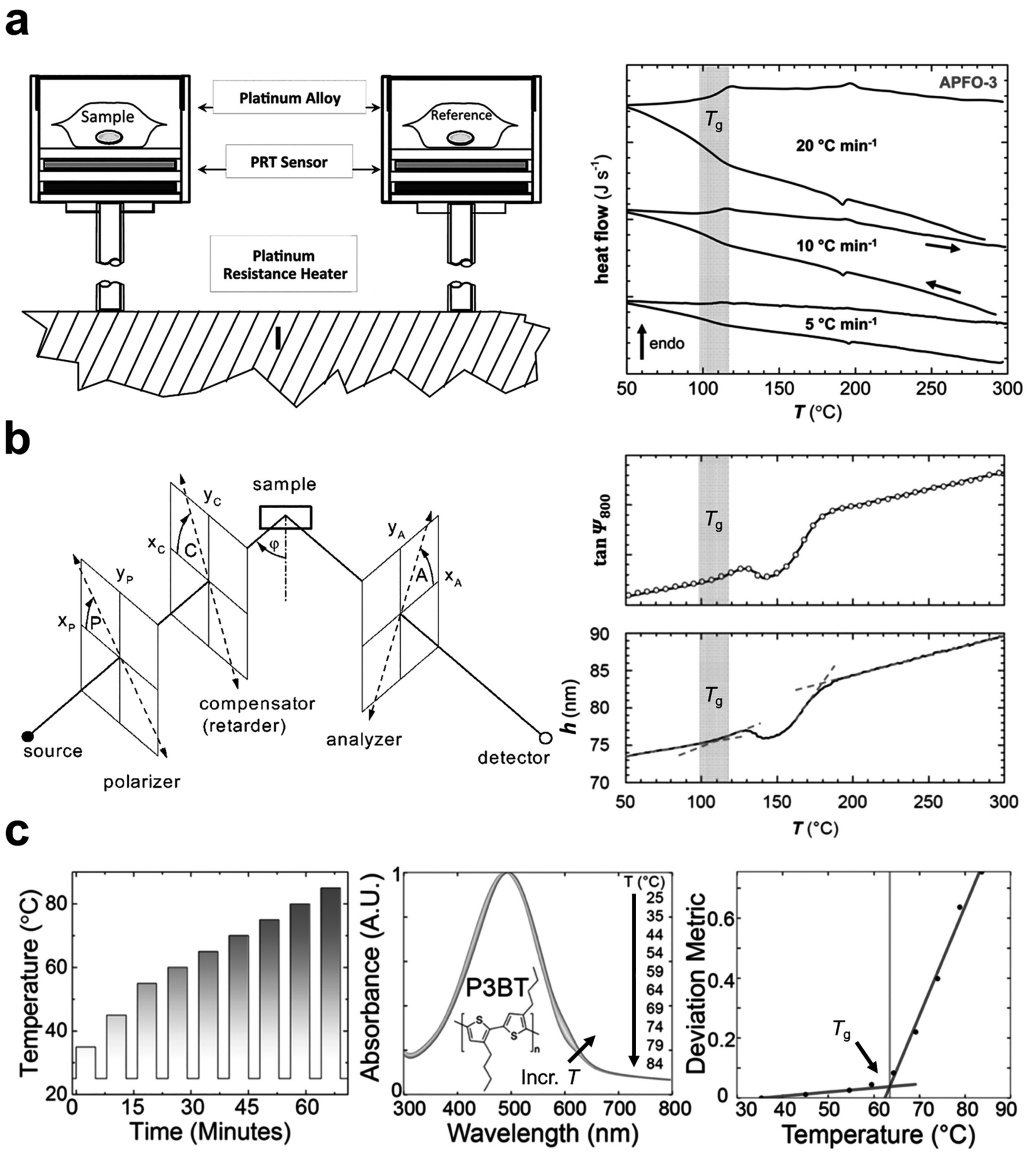

FIGURE 7.9 Experimental techniques to measure the T_g of a semiconducting polymer. (a, left) Schematic illustrating the main constituents of an original power compensation DSC; PRT stands for platinum resistance thermometer. Reproduced with permission from Gaisford et al., Royal Society of Chemistry, 2016. Copyright 2016, Royal Society of Chemistry. (a, right) Second DSC heating and cooling scans of a liquid–crystalline polyfluorene derivative (APFO-3) performed in an N_2 atmosphere at different scan rates. Reproduced with permission from Müller, *Chem. Mater.* 2015, 27, 2740–2754. Copyright 2015, American Chemical Society. (b, left) A typical ellipsometer comprises a polarizer, compensator, sample, and analyzer; a planar sample is assumed, and the angle of incidence is denoted by φ. Reproduced with permission from Tompkins et al., Springer, 2005. Copyright 2005, Elsevier. (b, right) Temperature dependence of the tan Ψ and h of a thin film of APFO-3 measured with VTE; the tan Ψ was measured at a wavelength of 800 nm, near which APFO-3 is optically transparent. Reproduced with permission from Müller et al., *J. Mater. Chem.* 2011, 21, 10676. Copyright 2011, Royal Society of Chemistry. (c) Measuring the T_g with UV–vis absorption spectroscopy involves (left) subjecting a thin film to a thermal cycling protocol, (center) recording the UV–vis spectrum of the film at ambient temperature between successive cycles, and (right) processing the spectra as a plot of the DM_T versus annealing temperature using Equation (7.6), the graph of which shows a distinct increase near the T_g. Reproduced with permission from Root et al., *Chem. Mater.* 2017, 29, 2646–2654. Copyright 2017, American Chemical Society.

Alternatively, VTE may be used to determine the T_g of a thin film by examining the dependence of the film's refractive index, n, and thickness, h, on temperature. Ellipsometry involves measuring the change in polarization—quantified by the amplitude ratio and phase shift—of elliptically polarized electromagnetic radiation reflected from the surface of a sample (Figure 7.9b, left). Ellipsometry is also used to noninvasively characterize the refractive indices and thicknesses of thin films of polymers. The thermal transitions of these materials can be quantified using an ellipsometer in conjunction with a temperature-controlled stage. For this measurement, the amplitude ratio (or ellipsometric angle), tan Ψ, is evaluated as a function of temperature,[69] which then allows determination of the refractive index and thickness as functions of temperature. The T_g can be approximated as a change in the slope of a graph of refractive index or thickness versus temperature,[70] which is related to the expansion of free volume above the T_g and, concurrently, an abrupt change in the volumetric coefficient of thermal expansion α_v:

$$\alpha_v = -\frac{1}{\rho}\left(\frac{d\rho}{dT}\right) = -\frac{V}{m}\left(\frac{d(m/V)}{dT}\right) \tag{7.4}$$

where ρ is density and m is the mass of a thin film of volume V.[66] Assuming that a laterally constrained film of a given area has a fixed mass of polymer, Equation (7.4) may be rewritten as

$$\alpha_v \approx -h\left(\frac{d(1/h)}{dT}\right) = \frac{1}{h}\left(\frac{dh}{dT}\right) \tag{7.5}$$

using the chain rule. Therefore, an abrupt change in α_v at the T_g corresponds to a distinct variation in the rate of change of h with T, as shown in Figure 7.9b (right). Although the T_g of thin films of semiconducting polymers can be extracted from the raw data, ellipsometric systems equipped with temperature-controlled stages are often expensive and not widely available.

A more widely available measurement technique that allows for the determination of the T_g uses a hot plate in an N_2-atmosphere glovebox and a UV–vis spectrometer. UV–vis spectroscopy normally involves radiation with wavelengths between 200 and 800 nm. Irradiated molecules containing π- or non-bonding electrons can absorb the energy to promote electronic transitions: the smaller the bandgap, the less energy is needed to excite electrons, and thus the longer the wavelength of radiation they absorb. Thermal annealing of thin films of semiconducting polymers in the solid state can result in self-assembly and aggregation into densely packed morphologies.[71] The formation of such strong interactions between chains can result in large redshifts[9,72] (i.e., an increase in wavelength) in the UV–vis absorption spectrum because of a reduction in the optical bandgap. The magnitude of the redshift, however, depends on the degree of order imposed on the polymer.[72] Measurement of the T_g with UV–vis spectroscopy, therefore, works best for materials with a strong propensity to form ordered photophysical aggregates upon thermal annealing. The T_g of a thin film of semiconducting polymer could be measured by quantifying the change in the absorption spectrum that results from a systematic protocol of thermal annealing (Figure 7.9c, left and center).[9] A deviation metric, DM_T, may then be defined as the sum of the squared deviations in the absorbance between as-cast films (at room temperature, T_R) and annealed films (at annealing temperature, T):

$$DM_T \equiv \sum_{\lambda_{min}}^{\lambda_{max}} [I_{T_R}(\lambda) - I_T(\lambda)]^2 \tag{7.6}$$

where λ is the wavelength, λ_{min} and λ_{max} are the lower and upper bounds of the optical sweep, respectively, and $I_{T_R}(\lambda)$ and $I_T(\lambda)$ are the normalized absorption intensities of the as-cast and annealed films, respectively. Approaching the T_g, a sharp increase in the slope of the DM_T when plotted against T occurs because of the activation of chain motion in the solid state.[9] Figure 7.9c (right) illustrates the evolution of the deviation metric as a function of annealing temperature for a thin film of poly(3-butylthiophene)

(P3BT)—the deviation metric shows a distinct increase near the T_g. Rigorous bilinear regression analysis based on a custom R^2-maximization algorithm is recommended to accurately estimate the T_g (such an algorithm is available in an open-sourced format).[9]

7.7 Theoretical Modeling

From a theoretical perspective, semiconducting polymers represent a mechanically unique class of polymers. The uniqueness arises in large part due to geometric constraints imposed by π-conjugation along the backbone. A theoretical foundation for describing semiconducting polymers is provided by many of the models reported in the extensive body of literature on the mechanical behavior of non-conjugated polymers. When considering mechanical properties, however, there are several attributes specific to semiconducting polymers that distinguish them from their non-conjugated counterparts. These attributes are a manifestation of nanoscale characteristics—such as the planarizing effects of π-conjugation along the backbone and the flexibility of side chains—and device-level considerations—such as film thickness and solid-state morphology. Existing theoretical treatments thus range from atomistic molecular dynamics of mechanisms of nanoscale deformation to continuum-scale modeling of the mechanical behavior of films of semicrystalline polymers.

7.7.1 Molecular Structure and Atomistic Simulations

The molecular structure of repeat units along a polymer chain is the first consideration for the overall mechanical behavior. The static geometry of these repeat units can be computed approximately using the well-developed numerical methods of quantum chemistry.[76–78] While density functional theory can yield reliable predictions of molecular geometry (Figure 7.10a), it falls short, in comparison to perturbation-based methods, when it comes to calculations of energy.[76,77] Moreover, the methods of

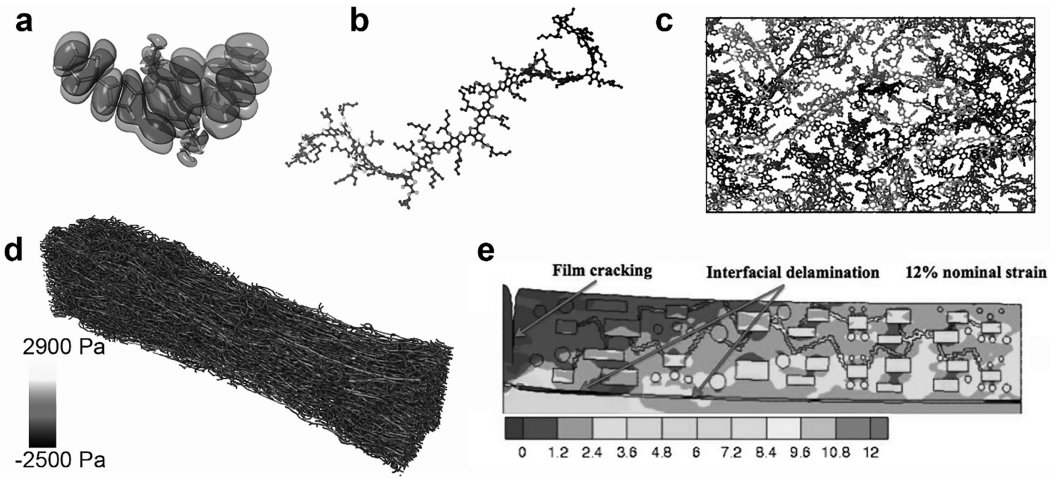

FIGURE 7.10 Theoretical and computational modeling of the mechanical properties of semiconducting polymers. (a) Illustration showing the highest-occupied molecular orbital (HOMO) of a diketopyrrolopyrrole (DPP) repeat unit obtained using density functional theory calculations. (b) Classical atomistic representation of a donor–acceptor polymer comprising branched alkyl side chains. (c) Atomistic simulations of a bulk donor–acceptor polymer under tensile strain; individual chains are colored distinctly. (d) A coarse-grained simulation of a P3HT film of high molecular weight subjected to tensile loading; polymer chains are colored based on their relative virial stress. (e) Multi-phase finite element simulation of a semicrystalline film of P3HT under tensile strain; the color scheme represents normalized normal stress. Reproduced with permission from Zhao et al., *J. Polym. Sci., Part B: Polym. Phys*. 2016, 54, 896–907. Copyright 2016, Wiley Periodicals, Inc.

computational quantum mechanics are too computationally expensive to describe the dynamics of even oligomeric chain segments, such that classical atomistic molecular dynamics must be employed.

Atomistic molecular dynamics simulations of semiconducting polymers generally use semi-empirical molecular force fields.[80,81] For conjugated polymers with complex backbone structures, many of the specific geometric, electrostatic, and energetic parameters must be obtained using quantum mechanical methods.[76,77] These parameters are typically associated with the planarizing intramolecular forces that exist between conjugated heterocyclic ring structures, such as dihedral rotations and bond stretches. The forces that control such molecular rotations are important in determining the time and temperature scales of stress relaxation through motion of polymer chains. These forces also influence the overall conformational structure of polymer chains, which subsequently determines the degree of their entanglement. Atomistic models based on classical, semi-empirical force fields are only capable of describing ground-state dynamics, neglecting mechanical effects of higher order that may arise due to excited-state and charge-transfer processes. (Mechanical effects of higher order include changes in molecular geometry that minimize electrostatic potential energy in the presence of charged species: namely electrons and holes. Ground-state dynamics, however, usually overwhelm these effects.) Furthermore, these models do not allow for the possibility of scission of chemical bonds; such a description is difficult from a numerical perspective because breakage of covalent bonds is associated with a large release of energy. Nevertheless, atomistic models provide practical predictions of the conformational preferences (Figure 7.10b), nanoscale packing features, and tensile behavior of complex donor–acceptor polymers (Figure 7.10c).

7.7.2 Polymer-Chain Size and Phase Behavior

The next length scale of interest is the size of polymer chains, which, combined with the chemical structure of the monomer, determines the overall phase behavior during solution casting. Conjugated polymers embody a wide range of behaviors in the solution phase, among which is the formation of single-chain and multi-chain aggregates.[76,82–85] The tendency to form such aggregates is important with regard to the mechanical stability of thin films processed from solution, as it leads to the creation of voids and lower densities of entanglement in the solid state.[8] This outcome is especially true for materials that undergo a glass transition well above room temperature and lack molecular mechanisms to relax kinetically trapped conformations without treatment by thermal annealing or solvent vapor. The solid-state morphology and tensile behavior of conjugated homopolymers, such as P3HT,[45,86] and numerous low-bandgap, alternating copolymers[8] have been studied in atomistic detail using modified force fields. An illustration of one such atomistic simulation is shown in Figure 7.10c.

Atomistic molecular dynamics simulations employ periodic boundary conditions and are thus used to model bulk samples. The stress–strain behavior of a bulk sample can be computed by imposing a constant strain rate in one dimension of the simulation box, and then by calculating the bulk stress in the axial dimension as the sum of all virial stresses acting on the particles. Atomistic simulations also provide predictions of packing at the molecular scale, tendency for entanglement, and mechanisms of deformation in semiconducting polymers of low molecular weight under tension. In addition, these simulations can be used to predict thermal properties, such as the glass transition temperature, by quenching a system from the melt phase and determining the temperature at which the coefficient of thermal expansion exhibits a change in slope. Atomistic simulations, however, do not consider any aspects of casting from solution and cannot be run long enough for crystallization to occur. In this regard, atomistic simulations can only be used to model the amorphous phase that is obtained by quenching from an equilibrated melt phase.

7.7.3 Coarse-Grained Simulations and Continuum-Based Methods

Although atomistic models can be used to describe the dynamics and mechanical behavior of systems of low molecular weight, the large length and time scales associated with polymers of high molecular weight

make these simulations computationally prohibitive. For such large scales, coarse-grained models must be employed. In these models of comparatively low resolution, groups of atoms are mapped to "beads" that have prescribed interactions and are optimized to match the results of atomistic simulations in either a melt or solution phase.[87–94] This coarse-graining procedure allows for the simulation of solution casting and may also be used to model a thin film in its entirety, such as the one shown in Figure 7.10d. These models have been employed to predict the mechanical behavior of P3ATs of high molecular weight and composite systems with fullerene molecules. Such simulations show reliable predictions of the tensile modulus, Poisson ratio, and glass transition temperature.[4,30] In addition, alignment of polymer chains due to plastic deformation and stress concentration within chains can be calculated (see Figure 7.10d). Finally, important theoretical properties, such as the density of entanglements, can be computed directly from coarse-grained simulations using algorithms of primitive-path analysis developed for non-conjugated polymers.[43,95–97] One particularly insightful observation that emerged from these simulations is that P3HT chains tend to fold on themselves when mixed with fullerenes.[10] This folding leads to a reduction in entanglement between chains and, consequently, a decrease in the toughness of the composite material.

For simulations of even larger scale that include bulk, semicrystalline domains, continuum-based methods must be employed. Finite element simulations consisting of three-phase heterogeneous models for P3HT have been developed to account for the crystallinity of ordered regions, elasto-viscoplasticity of amorphous regions, and even hypo-elasticity of tie chains between interconnected crystalline domains.[79,98] A typical simulation output that depicts the concentration of stress in a representative semicrystalline morphology is shown in Figure 7.10e. Although these simulations can provide detailed mechanisms of deformation that agree well with experiment, they require numerous mechanical parameters that are not known for most semiconducting polymers.

7.8 Composite Systems

The importance of composite systems is exemplified by the bulk heterojunction (BHJ)—an intimate blend of two or more semiconducting components—which functions as the active layer in organic solar cells. This structure introduces additional challenges to understanding the deformability of semiconducting polymers because the mechanical properties of a composite depend not only on those of its constituents but also on complex interactions between these components.

7.8.1 Effects of Molecular Mixing

In a BHJ, the electron donor is typically a semiconducting polymer and the electron acceptor may be a fullerene derivative.[99] In electron-donating polymers, side chains can have a high attachment density such as in P3HT, where each thiophene ring has a side chain attached. On the other hand, side chains could be sparse such as in poly(2,5-bis(3-tetradecyllthiophen-2-yl)thieno[3,2-*b*]thiophene) (PBTTT), where individual thiophene rings with side chains attached are separated by naked thienothiophene units. In polymers that exhibit lower attachment densities of side chains, greater free volume exists, which allows for the intercalation of fullerene crystals between the side chains. This intercalation results in a mixed, bimolecular blend where fullerene molecules can directly interact with the polymer backbone.[100]

When mixed with [60]PCBM, P3ATs generally do not allow for [60]PCBM intercalation, whereas PBTTTs and poly(terthiophenes) (e.g., poly-2,2′:5′,2″-(3,3″-dihexyl-terthiophene) (PT2T)) do (Figure 7.11a).[101] P3AT:fullerene blends, mixed in ratios of 1:1, form ternary morphologies that comprise fullerene-rich domains, polymer-rich aggregates, and a mixed, amorphous phase.[102] Moreover, PBTTT:fullerene blends form a bimolecular phase that is well-ordered (i.e., bimolecular crystallites),[103] while the bimolecular phase of PT2T:fullerene blends is disordered. The latter may be inferred based on the disappearance of the vibronic peaks in the UV–vis absorption spectrum of PT2T upon adding [60]PCBM,

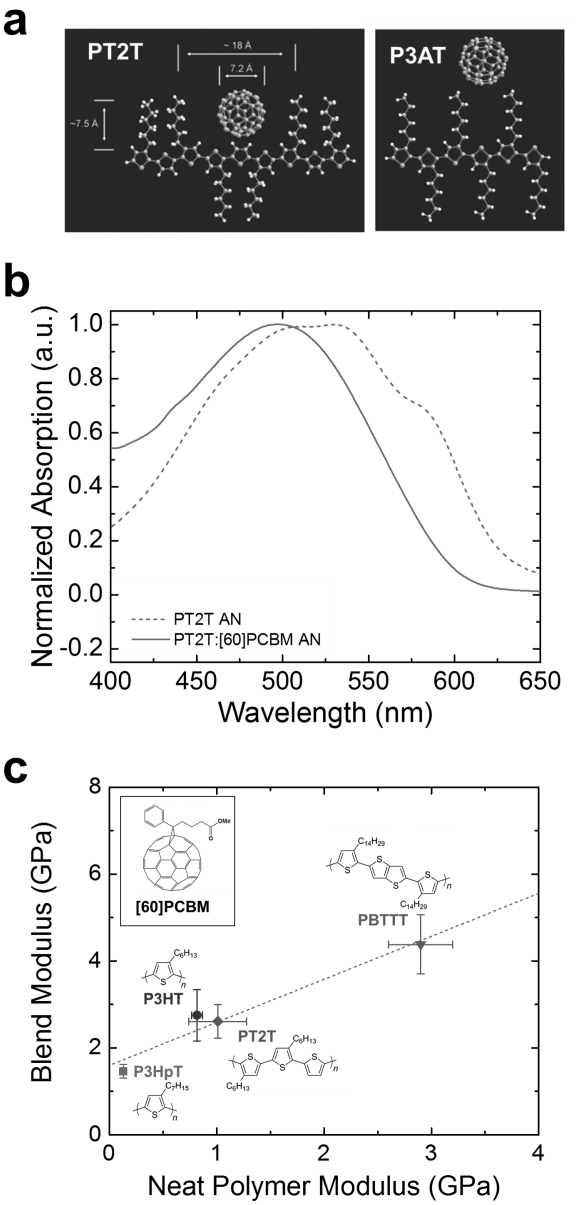

FIGURE 7.11 Effects of fullerene mixing on semiconducting polymers. (a) C_{60} can readily intercalate along the backbone of polymers that are structurally similar to PT2T, which has side chains that are sparsely attached, but it cannot intercalate along the backbone of polymers that are structurally similar to P3ATs, which have side chains that are densely attached. Reproduced with permission from Koppe et al., *Adv. Funct. Mater.* 2007, 17, 1371–1376. Copyright 2007, Wiley-VCH Verlag, GmbH & Co. KGaA. (b) UV–vis absorption spectra of neat PT2T and PT2T:[60]PCBM (both thermally annealed) showing the disruption of PT2T ordering—as suggested by the complete vanishing of the vibronic peaks—upon addition of [60]PCBM. (c) Linear correlation between the elastic moduli of polymer:fullerene blends and those of the corresponding neat polymers. Reproduced with permission from Printz et al., *Sol. Energy Mater. Sol. Cells* 2015, 134, 64–72. Copyright 2015, Elsevier.

as shown in Figure 7.11b.[104] (Vibronic peaks in a UV–vis absorption spectrum are indicative of polymer aggregation, such that their disappearance corresponds to a disruption in microstructural order.) An important consequence of molecular mixing is thus that the elastic moduli of polymer:fullerene blends are lower than simple averages of the moduli of the individual components. As shown in Figure 7.11c, a linear correlation may nevertheless be observed between the moduli of blends and those of the corresponding neat polymers.[104]

7.8.2 Polymer–Fullerene Composites

Methanofullerenes are fullerene derivatives commonly used as the electron-accepting component of a BHJ and, mechanically, are extremely brittle van der Waals solids. In general, fullerenes are produced as a mixture of various structures, though their separation is a resource-intensive and energetically expensive process.[105] Two common methanofullerenes are [60]PCBM, which comprises a spherical 60-carbon fullerene and a solubilizing side chain, and [6,6]-phenyl C_{71} butyric acid methyl ester ([70]PCBM), which comprises an ovoidal 70-carbon fullerene but has the same solubilizing side chain as in [60]PCBM (Figure 7.12a). The former packs efficiently and readily crystallizes to the point that it fractures at very low strain. On the other hand, [70]PCBM can withstand slightly more deformation because it packs less efficiently and is morphologically hindered due to its ovoidal shape and numerous isomers.[106] The mechanical stability of organic semiconductors, however, is determined not only by molecular structure

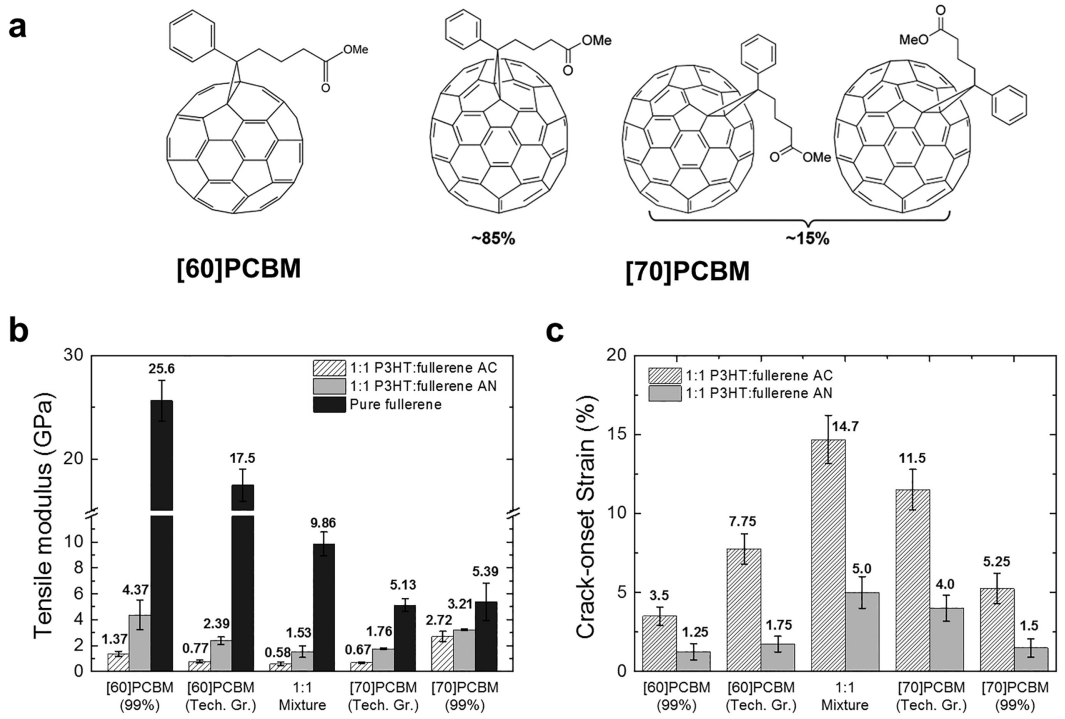

FIGURE 7.12 Effects of fullerene mixing on semiconducting polymers. (a) Molecular structures of [60]PCBM and [70]PCBM; the latter is predominantly a mixture of three different isomers. (b) Tensile moduli of polymer:fullerene composites as functions of the relative concentrations of [60]PCBM and [70]PCBM. Data for pure fullerene films and their respective composites, as-cast (AC) and after thermal annealing (AN), are included. Compared to composites with separated fullerenes, composites with mixed fullerenes exhibit lower elastic moduli and (c) higher crack-onset strains. Reproduced with permission from Savagatrup et al., *Chem. Mater.* 2015, 27, 3902–3911. Copyright 2015, American Chemical Society.

but also by the solid-state morphology of the film.[107] Methanofullerenes behave as anti-plasticizers when mixed with semiconducting polymers by increasing the glass transition temperature and elastic modulus and by reducing the strain at fracture and cohesive energy.[6,106,108] These effects on the thermomechanical properties of semiconducting polymers all result in more fragile polymer:fullerene systems overall.

The detrimental effects that [60]PCBM and [70]PCBM have on the mechanical performance of semiconducting polymers indicate that these fullerene derivatives, individually, are far from ideal electron acceptors for low-cost applications that require mechanical durability. Nonetheless, incompletely separated fullerenes combine the advantage of a lower embodied energy—i.e., the total input of energy for synthesis and processing of fullerenes—with a reduction in modulus and an increase in crack-onset strain.[106] Increases in compliance and extensibility, as shown in Figure 7.12b and Figure 7.12c, can be attributed to synergy between the inefficient packing of fullerene molecules in fullerene-rich domains and a reduction in polymer aggregation.[106] BHJ blends that comprise incompletely separated fullerenes, though still stiffer and more brittle than the polymeric component alone, exhibit greater deformability compared to BHJs consisting of completely separated fullerenes.[106] Thermal annealing of these blends, particularly those comprising polythiophene-based polymers, induces molecular aggregation and crystallization.[12] This improved molecular ordering, however, stiffens and embrittles the films, as demonstrated in Figure 7.12b and Figure 7.12c.[46,106]

7.9 Conclusion and Outlook

Mechanical deformability is the characteristic that enables most touted advantages of organic electronic materials. Although the field of flexible and robust electronics is nascent with as of yet few commercialized products, significant efforts to determine how chemical structure and microstructural order influence the mechanical properties of semiconducting polymers have already been made. The mechanical properties of thin films of semiconducting polymers depend on molecular structure and also on molecular packing in the solid state. Indeed, a recurring finding, both experimentally and computationally, is that the thermomechanical properties of semiconducting polymers are controlled by conditions of solution and thermal processing, which directly influence crystallinity and nanoscale ordering. A complete understanding of the mechanical properties of these materials entails developing a framework for how specific molecular structures assemble in solution and ultimately in the solid state.

Determining the mechanical properties of thin films has proven difficult in numerous ways, primarily due to the impracticality of handling these materials in freestanding form. These challenges have led to the development of broadly applicable approaches to metrology, such as the film-on-elastomer and film-on-water methods, that can be readily applied to semiconducting polymers. Although these techniques allow for facile determination of the mechanical properties of thin films, the results of such mechanical analyses are dependent on the technique and testing conditions used. Another typical complication in characterizing the mechanical properties of thin films of semiconducting polymer lies in the diversity of the fracture behavior that these materials exhibit. In addition, the mechanics that govern ductile fracture—compared to brittle fracture—are more sophisticated and less well understood due to the occurrence of plastic flow during events of ductile fracture.

A deeper understanding of the mechanical properties of semiconducting polymers will enable the production of organic electronics that are mechanically robust and resistant to fracture. For these devices to be a technological success, however, efforts to enhance their thermomechanical properties and long-term reliability against mechanical deformation must not come second to optimizing electronic performance. Instead, the primary objective in developing robust and efficient devices should be to co-optimize the mechanical and optoelectronic properties of semiconducting polymers. For this purpose, computational methods and theoretical modeling are expected to play a crucial role in facilitating the co-optimization of mechanical and electronic properties by generating experimentally testable hypotheses. These efforts directed toward an improved understanding of the thermomechanical properties of semiconducting polymers may also reveal ways in which to create materials with properties

inspired by biological tissue, including simultaneous toughness and compliance, degradability, and the capacity to self-repair.

References

1. Xu, J. M. Plastic Electronics and Future Trends in Microelectronics. *Synth. Met.* 2000, *115*, 1–3.
2. Wong, W. S., Salleo, A., Eds. *Flexible Electronics: Materials and Applications*, 1st ed.; Springer Science & Business Media, 2009.
3. Facchetti, A. π-Conjugated Polymers for Organic Electronics and Photovoltaic Cell Applications. *Chem. Mater.* 2011, *23*, 733–758.
4. Root, S. E.; Savagatrup, S.; Printz, A. D.; Rodriquez, D.; Lipomi, D. J. Mechanical Properties of Organic Semiconductors for Stretchable, Highly Flexible, and Mechanically Robust Electronics. *Chem. Rev.* 2017, *117*, 6467–6499.
5. Mei, J.; Bao, Z. Side Chain Engineering in Solution-Processable Conjugated Polymers. *Chem. Mater.* 2014, *26*, 604–615.
6. Savagatrup, S.; Printz, A. D.; Wu, H.; Rajan, K. M.; Sawyer, E. J.; Zaretski, A. V.; Bettinger, C. J.; Lipomi, D. J. Viability of Stretchable Poly(3-Heptylthiophene) (P3HpT) for Organic Solar Cells and Field-Effect Transistors. *Synth. Met.* 2015, *203*, 208–214.
7. Müller, C. On the Glass Transition of Polymer Semiconductors and Its Impact on Polymer Solar Cell Stability. *Chem. Mater.* 2015, *27*, 2740–2754.
8. Root, S. E.; Jackson, N.; Savagatrup, S.; Arya, G.; Lipomi, D. J. Modelling the Morphology and Thermomechanical Behaviour of Low-Bandgap Conjugated Polymers and Bulk Heterojunction Films. *Energy Environ. Sci.* 2016, *10*, 558–569.
9. Root, S. E.; Alkhadra, M. A.; Rodriquez, D.; Printz, A. D.; Lipomi, D. J. Measuring the Glass Transition Temperature of Conjugated Polymer Films with Ultraviolet-Visible Spectroscopy. *Chem. Mater.* 2017, *29*, 2646–2654.
10. Root, S. E.; Savagatrup, S.; Pais, C. J.; Arya, G.; Lipomi, D. J. Predicting the Mechanical Properties of Organic Semiconductors Using Coarse-Grained Molecular Dynamics Simulations. *Macromolecules* 2016, *49*, 2886–2894.
11. Capaldi, F. M.; Boyce, M. C.; Rutledge, G. C. Molecular Response of a Glassy Polymer to Active Deformation. *Polymer* 2004, *45*, 1391–1399.
12. O'Connor, B.; Chan, E. P.; Chan, C.; Conrad, B. R.; Richter, L. J.; Kline, R. J.; Heeney, M.; McCulloch, I.; Soles, C. L.; DeLongchamp, D. M. Correlations between Mechanical and Electrical Properties of Polythiophenes. *ACS Nano* 2010, *4*, 7538–7544.
13. Ward, I. M.; Sweeney, J. *Mechanical Properties of Solid Polymers*, 3rd ed.; John Wiley & Sons, 2012.
14. Alkhadra, M. A.; Root, S. E.; Hilby, K. M.; Rodriquez, D.; Sugiyama, F.; Lipomi, D. J. Quantifying the Fracture Behavior of Brittle and Ductile Thin Films of Semiconducting Polymers. *Chem. Mater.* 2017, *29*, 10139–10149.
15. Balar, N.; O'Connor, B. T. Correlating Crack Onset Strain and Cohesive Fracture Energy in Polymer Semiconductor Films. *Macromolecules* 2017, *50*, 8611–8618.
16. Tong, T.; Babatope, B.; Admassie, S.; Meng, J.; Akwogu, O.; Akande, W.; Soboyejo, W. O. Adhesion in Organic Electronic Structures. *J. Appl. Phys.* 2009, *106*, 083708.
17. Karagiannidis, P. G.; Kassavetis, S.; Pitsalidis, C.; Logothetidis, S. Thermal Annealing Effect on the Nanomechanical Properties and Structure of P3HT:PCBM Thin Films. *Thin Solid Films* 2011, *519*, 4105–4109.
18. Kim, J.-H.; Nizami, A.; Hwangbo, Y.; Jang, B.; Lee, H.-J.; Woo, C.-S.; Hyun, S.; Kim, T.-S. Tensile Testing of Ultra-Thin Films on Water Surface. *Nat. Commun.* 2013, *4*, 2520.
19. Printz, A. D.; Zaretski, A. V.; Savagatrup, S.; Chiang, A. S.-C.; Lipomi, D. J. Yield Point of Semiconducting Polymer Films on Stretchable Substrates Determined by Onset of Buckling. *ACS Appl. Mater. Interfaces* 2015, *7*, 23257–23264.

20. Dupont, S. R.; Voroshazi, E.; Heremans, P.; Dauskardt, R. H. Adhesion Properties of Inverted Polymer Solarcells: Processing and Film Structure Parameters. *Org. Electron.* 2013, *14*, 1262–1270.
21. Kim, T.; Kim, J.-H.; Kang, T. E.; Lee, C.; Kang, H.; Shin, M.; Wang, C.; Ma, B.; Jeong, U.; Kim, T.-S.; Kim, B. J. Flexible, Highly Efficient All-Polymer Solar Cells. *Nat. Commun.* 2015, *6*, 8547.
22. Stafford, C. M.; Harrison, C.; Beers, K. L.; Karim, A.; Amis, E. J.; VanLandingham, M. R.; Kim, H. C.; Volksen, W.; Miller, R. D.; Simonyi, E. E. A Buckling-Based Metrology for Measuring the Elastic Moduli of Polymeric Thin Films. *Nat. Mater.* 2004, *3*, 545–550.
23. Rodriquez, D.; Savagatrup, S.; Valle, E.; Proctor, C. M.; McDowell, C.; Bazan, G. C.; Nguyen, T.-Q.; Lipomi, D. J. Mechanical Properties of Solution-Processed Small-Molecule Semiconductor Films. *ACS Appl. Mater. Interfaces* 2016, *8*, 11649–11657.
24. Volynskii, A. L.; Bazhenov, S.; Lebedeva, O. V.; Bakeev, N. F. Mechanical Buckling Instability of Thin Coatings Deposited on Soft Polymer Substrates. *J. Mater. Sci.* 2000, *35*, 547–554.
25. Roth, B.; Savagatrup, S.; De Los Santos, N. V.; Hagemann, O.; Carlé, J. E.; Helgesen, M.; Livi, F.; Bundgaard, E.; Søndergaard, R. R.; Krebs, F. C.; Lipomi, D. J. Mechanical Properties of a Library of Low-Band-Gap Polymers. *Chem. Mater.* 2016, *28*, 2363–2373.
26. Dundurs, J. Elastic Interaction of Dislocations with Inhomogeneities. In *Mathematical Theory of Dislocations*; Mura, T., Ed.; American Society of Mechanical Engineers, 1969; pp. 70–115.
27. Beuth, J. L. Cracking of Thin Bonded Films in Residual Tension. *Int. J. Solids Struct.* 1992, *29*, 1657–1675.
28. Xia, Z. C.; Hutchinson, J. W. Crack Patterns in Thin Films. *J. Mech. Phys. Solids* 2000, *48*, 1107–1131.
29. Li, T.; Huang, Z.; Suo, Z.; Lacour, S. P.; Wagner, S. Stretchability of Thin Metal Films on Elastomer Substrates. *Appl. Phys. Lett.* 2004, *85*, 3435–3437.
30. Rodriquez, D.; Kim, J.-H.; Root, S. E.; Fei, Z.; Boufflet, P.; Heeney, M.; Kim, T.-S.; Lipomi, D. J. Comparison of Methods for Determining the Mechanical Properties of Semiconducting Polymer Films for Stretchable Electronics. *ACS Appl. Mater. Interfaces* 2017, *9*, 8855–8862.
31. Lu, N.; Wang, X.; Suo, Z.; Vlassak, J. Metal Films on Polymer Substrates Stretched Beyond 50%. *Appl. Phys. Lett.* 2007, *91*, 221909.
32. Sawyer, E. J.; Zaretski, A. V.; Printz, A. D.; de los Santos, N. V.; Bautista-Gutierrez, A.; Lipomi, D. J. Large Increase in Stretchability of Organic Electronic Materials by Encapsulation. *Extrem. Mech. Lett.* 2016, *8*, 78–87.
33. Bruner, C.; Dauskardt, R. Role of Molecular Weight on the Mechanical Device Properties of Organic Polymer Solar Cells. *Macromolecules* 2014, *47*, 1117–1121.
34. Keddie, J. L.; Jones, R. A. L.; Cory, R. A. Size-Dependent Depression of the Glass Transition Temperature in Polymer Films. *Europhys. Lett.* 1994, *27*, 59–64.
35. Wang, T.; Pearson, A. J.; Dunbar, A. D. F.; Staniec, P. A.; Watters, D. C.; Coles, D.; Yi, H.; Iraqi, A.; Lidzey, D. G.; Jones, R. A. L. Competition between Substrate-Mediated π-π Stacking and Surface-Mediated T_g Depression in Ultrathin Conjugated Polymer Films. *Eur. Phys. J. E. Soft Matter* 2012, *35*, 9807.
36. Si, L.; Massa, M. V.; Dalnoki-Veress, K.; Brown, H. R.; Jones, R. A. L. Chain Entanglement in Thin Freestanding Polymer Films. *Phys. Rev. Lett.* 2005, *94*, 127801.
37. Liu, D.; Orozco, R. O.; Wang, T. Deviations of the Glass Transition Temperature in Amorphous Conjugated Polymer Thin Films. *Phys. Rev. E* 2013, *88*, 022601.
38. Zhao, J.-H.; Kiene, M.; Hu, C.; Ho, P. S. Thermal Stress and Glass Transition of Ultrathin Polystyrene Films. *Appl. Phys. Lett.* 2000, *77*, 2843.
39. Lee, J. H.; Chung, J. Y.; Stafford, C. M. Effect of Confinement on Stiffness and Fracture of Thin Amorphous Polymer Films. *ACS Macro Lett.* 2012, *1*, 122–126.
40. Mulliken, A. D.; Boyce, M. C. Mechanics of the Rate-Dependent Elastic-Plastic Deformation of Glassy Polymers from Low to High Strain Rates. *Int. J. Solids Struct.* 2006, *43*, 1331–1356.
41. Richeton, J.; Ahzi, S.; Vecchio, K. S.; Jiang, F. C.; Adharapurapu, R. R. Influence of Temperature and Strain Rate on the Mechanical Behavior of Three Amorphous Polymers: Characterization and Modeling of the Compressive Yield Stress. *Int. J. Solids Struct.* 2006, *43*, 2318–2335.

42. Koch, F. P. V.; Rivnay, J.; Foster, S.; Müller, C.; Downing, J. M.; Buchaca-Domingo, E.; Westacott, P.; Yu, L.; Yuan, M.; Baklar, M.; Fei, Z.; Luscombe, C.; Mclachlan, M. A.; Heeney, M.; Rumbles, G.; Silva, C.; Salleo, A.; Nelson, J.; Smith, P.; Stingelin, N.The Impact of Molecular Weight on Microstructure and Charge Transport in Semicrystalline Polymer Semiconductors–Poly(3-Hexylthiophene), a Model Study. *Prog. Polym. Sci.* 2013, 38, 1978–1989.
43. Shanbhag, S.; Kröger, M. Primitive Path Networks Generated by Annealing and Geometrical Methods: Insights into Differences. *Macromolecules* 2007, *40*, 2897–2903.
44. Kröger, M. Shortest Multiple Disconnected Path for the Analysis of Entanglements in Two- and Three-Dimensional Polymeric Systems. *Comput. Phys. Commun.* 2005, *168*, 209–232.
45. Tummala, N. R.; Bruner, C.; Risko, C.; Brédas, J.-L.; Dauskardt, R. H. Molecular-Scale Understanding of Cohesion and Fracture in P3HT:Fullerene Blends. *ACS Appl. Mater. Interfaces* 2015, *7*, 9957–9964.
46. Savagatrup, S.; Printz, A. D.; Rodriquez, D.; Lipomi, D. J. Best of Both Worlds: Conjugated Polymers Exhibiting Good Photovoltaic Behavior and High Tensile Elasticity. *Macromolecules* 2014, *47*, 1981–1992.
47. Savagatrup, S.; Makaram, A. S.; Burke, D. J.; Lipomi, D. J. Mechanical Properties of Conjugated Polymers and Polymer-Fullerene Composites as a Function of Molecular Structure. *Adv. Funct. Mater.* 2014, *24*, 1169–1181.
48. Savagatrup, S.; Printz, A. D.; O'Connor, T. F.; Zaretski, A. V.; Rodriquez, D.; Sawyer, E. J.; Rajan, K. M.; Acosta, R. I.; Root, S. E.; Lipomi, D. J. Mechanical Degradation and Stability of Organic Solar Cells: Molecular and Microstructural Determinants. *Energy Environ. Sci.* 2015, *8*, 55–80.
49. Koch, F. P. V.; Heeney, M.; Smith, P. Thermal and Structural Characteristics of Oligo(3-Hexylthiophene)s $(3HT)_n$, $n = 4–36$. *J. Am. Chem. Soc.* 2013, *135*, 13699–13709.
50. Yiu, A. T.; Beaujuge, P. M.; Lee, O. P.; Woo, C. H.; Toney, M. F.; Fréchet, J. M. J. Side-Chain Tunability of Furan-Containing Low-Band-Gap Polymers Provides Control of Structural Order in Efficient Solar Cells. *J. Am. Chem. Soc.* 2012, *134*, 2180–2185.
51. Ho, V.; Boudouris, B. W.; Segalman, R. A. Tuning Polythiophene Crystallization Through Systematic Side Chain Functionalization. *Macromolecules* 2010, *43*, 7895–7899.
52. Kim, J.-S.; Kim, J.-H.; Lee, W.; Yu, H.; Kim, H. J.; Song, I.; Shin, M.; Oh, J. H.; Jeong, U.; Kim, T.-S.; Kim, B. J. Tuning Mechanical and Optoelectrical Properties of Poly(3-Hexylthiophene) Through Systematic Regioregularity Control. *Macromolecules* 2015, *48*, 4339–4346.
53. Lipomi, D. J.; Chong, H.; Vosgueritchian, M.; Mei, J.; Bao, Z. Toward Mechanically Robust and Intrinsically Stretchable Organic Solar Cells: Evolution of Photovoltaic Properties with Tensile Strain. *Sol. Energy Mater. Sol. Cells* 2012, *107*, 355–365.
54. Zhao, Y.; Zhao, X.; Zang, Y.; Di, C. A.; Diao, Y.; Mei, J. Conjugation-Break Spacers in Semiconducting Polymers: Impact on Polymer Processability and Charge Transport Properties. *Macromolecules* 2015, *48*, 2048–2053.
55. Wu, H.-C.; Benight, S. J.; Chortos, A.; Lee, W.-Y.; Mei, J.; F To, J. W.; Lu, C.; He, M.; B-H Tok, J.; Chen, W.-C.; Bao, Z. A Rapid and Facile Soft Contact Lamination Method: Evaluation of Polymer Semiconductors for Stretchable Transistors. *Chem. Mater.* 2014, *36*, 4544–4551.
56. Savagatrup, S.; Zhao, X.; Chan, E.; Mei, J.; Lipomi, D. J. Effect of Broken Conjugation on the Stretchability of Semiconducting Polymers. *Macromol. Rapid Commun.* 2016, *27*, 1623–1628.
57. Liu, J.; Sun, Y.; Gao, X.; Xing, R.; Zheng, L.; Wu, S.; Geng, Y.; Han, Y. Oriented Poly(3-Hexylthiophene) Nanofibril with the π-π Stacking Growth Direction by Solvent Directional Evaporation. *Langmuir* 2011, *27*, 4212–4219.
58. Strobl G. *The Physics of Polymers: Concepts for Understanding Their Structures and Behavior*, 2nd ed.; Springer, 1997.
59. Gutzow, I. S.; Schmelzer, J. W. P. *The Vitreous State: Thermodynamics, Structure, Rheology, and Crystallization*, 2nd ed.; Springer, 2013.
60. Reimschuessel, H. K. Glass-Transition Temperature of Comblike Polymers: Effects of Side-Chain Length and Backbone Chain Structure. *J. Polym. Sci., Part A: Polym. Chem.* 1979, *17*, 2447–2457.

61. Cowie, J. M. G.; Reid, V. M. C.; Mcewen, I. J. Effect of Side Chain Length on the Glass Transition of Copolymers from Styrene with n-Alkyl Citraconimides and with n-Alkyl Itaconimides. *Br. Polym. J.* 1990, *23*, 353–357.
62. Bruner, C.; Novoa, F.; Dupont, S.; Dauskardt, R. Decohesion Kinetics in Polymer Organic Solar Cells. *ACS Appl. Mater. Interfaces* 2014, *6*, 21474–21483.
63. Haward, R. N., Young, R. J., Eds. *The Physics of Glassy Polymers*, 2nd ed.; Springer Science & Business Media, 1997.
64. Danley, R. L.; Reader, J. R.; Schaefer, J. W. Differential Scanning Calorimeter. U.S. Patent US5842788 A, 1998.
65. Rieger, J. Glass Transition Temperature T_g of Polymers-Comparison of the Values from Differential Thermal Analysis (DTA, DSC) and Dynamic Mechanical Measurements (Torsion Pendulum). *Polym. Test.* 2001, *20*, 199–204.
66. Beaucage, G.; Composto, R.; Stein, R. S. Ellipsometric Study of the Glass Transition and Thermal Expansion Coefficients of Thin Polymer Films. *J. Polym. Sci., Part B: Polym. Phys.* 1993, *31*, 319–326.
67. Wunderlich, B. Study of the Change in Specific Heat of Monomeric and Polymeric Glasses during the Glass Transition. *J. Phys. Chem.* 1960, *64*, 1052–1056.
68. Campoy-Quiles, M.; Sims, M.; Etchegoin, P. G.; Bradley, D. D. C. Thickness-Dependent Thermal Transition Temperatures in Thin Conjugated Polymer Films. *Macromolecules* 2006, *39*, 7673–7680.
69. McCrackin, F. L.; Passaglia, E.; Stromberg, R. R.; Steinberg, H. L. Measurement of the Thickness and Refractive Index of Very Thin Films and the Optical Properties of Surfaces by Ellipsometry. *J. Res. Natl. Inst. Stand. Technol.* 1963, *67A*, 363–377.
70. Parks, G. S.; Huffman, H. M.; Cattoir, F. R. Studies on Glass. II. The Transition between the Glassy and Liquid States in the Case of Glucose. *J. Phys. Chem.* 1928, *32*, 1366–1379.
71. Holliday, S.; Donaghey, J. E.; McCulloch, I. Advances in Charge Carrier Mobilities of Semiconducting Polymers Used in Organic Transistors. *Chem. Mater.* 2013, *26*, 647–663.
72. Kim, D. H.; Lee, B. L.; Moon, H.; Kang, H. M.; Jeong, E. J.; Park, J. Il; Han, K. M.; Lee, S.; Yoo, B. W.; Koo, B. W.; Kim, J. Y.; Lee, W. H.; Cho, K.; Becerril, H. A.; Bao, Z. Liquid-Crystalline Semiconducting Copolymers with Intramolecular Donor-Acceptor Building Blocks for High-Stability Polymer Transistors. *J. Am. Chem. Soc.* 2009, *131*, 6124–6132.
73. Gaisford, S., Kett, V., Haines, P., Eds. *Principles of Thermal Analysis and Calorimetry*, 2nd ed.; Royal Society of Chemistry, 2016.
74. Tompkins, H. G., Irene, E. A., Eds. *Handbook of Ellipsometry*, 1st ed.; Springer, 2005.
75. Müller, C.; Bergqvist, J.; Vandewal, K.; Tvingstedt, K.; Anselmo, A. S.; Magnusson, R.; Alonso, M. I.; Moons, E.; Arwin, H.; Campoy-Quiles, M.; Inganäs, O. Phase Behaviour of Liquid-Crystalline Polymer/Fullerene Organic Photovoltaic Blends: Thermal Stability and Miscibility. *J. Mater. Chem.* 2011, *21*, 10676.
76. Jackson, N. E.; Kohlstedt, K. L.; Savoie, B. M.; Olvera de la Cruz, M.; Schatz, G. C.; Chen, L. X.; Ratner, M. A. Conformational Order in Aggregates of Conjugated Polymers. *J. Am. Chem. Soc.* 2015, *137*, 6254–6262.
77. Dubay, K. H.; Hall, M. L.; Hughes, T. F.; Wu, C.; Reichman, D. R.; Friesner, R. A. Accurate Force Field Development for Modeling Conjugated Polymers. *J. Chem. Theory Comput.* 2012, *8*, 4556–4569.
78. Marcon, V.; Raos, G. Free Energies of Molecular Crystal Surfaces by Computer Simulation: Application to Tetrathiophene. *J. Am. Chem. Soc.* 2006, *128*, 1408–1409.
79. Zhao, B.; Awartani, O.; O'Connor, B.; Zikry, M. A. Microstructural Behavior and Failure Mechanisms of Organic Semicrystalline Thin Film Blends. *J. Polym. Sci., Part B: Polym. Phys.* 2016, *54*, 896–907.
80. Jorgensen, W. L.; Maxwell, D. S.; Tirado-Rives, J. Development and Testing of the OPLS All-Atom Force Field on Conformational Energetics and Properties of Organic Liquids. *J. Am. Chem. Soc.* 1996, *118*, 11225–11236.

81. Do, K.; Huang, D. M.; Moule, A. J. A Comparative MD Study of the Local Structure of Polymer Semiconductors P3HT and PBTTT. *Phys. Chem. Chem. Phys.* 2010, *12*, 14735–14739.
82. Schwarz, K. N.; Kee, T. W.; Huang, D. M. Coarse-Grained Simulations of the Solution-Phase Self-Assembly of Poly(3-Hexylthiophene) Nanostructures. *Nanoscale* 2013, *5*, 2017–2027.
83. Fauvell, T. J.; Zheng, T.; Jackson, N. E.; Ratner, M. A.; Yu, L.; Chen, L. X. The Photophysical and Morphological Implications of Single-Strand Conjugated Polymer Folding in Solution. *Chem. Mater.* 2016, *28*, 2814–2822.
84. Stewart, B.; Burrows, H. Molecular Dynamics Study of Self-Assembly of Aqueous Solutions of Poly[9,9-bis(4-Sulfonylbutoxyphenylphenyl) Fluorene-2,7-Diyl-2,2′-Bithiophene] (PBS-PF2T) in the Presence of Pentaethylene Glycol Monododecyl Ether ($C_{12}E_5$). *Materials* 2016, *9*, 379.
85. Newbloom, G. M.; Hoffmann, S. M.; West, A. F.; Gile, M. C.; Sista, P.; Cheung, H. K. C.; Luscombe, C. K.; Pfaendtner, J.; Pozzo, L. D. Solvatochromism and Conformational Changes in Fully Dissolved Poly(3-Alkylthiophene)s. *Langmuir* 2015, *31*, 458–468.
86. Tummala, N. R.; Risko, C.; Bruner, C.; Dauskardt, R. H.; Brédas, J.-L. Entanglements in P3HT and Their Influence on Thin-Film Mechanical Properties: Insights from Molecular Dynamics Simulations. *J. Polym. Sci., Part B: Polym. Phys.* 2015, *53*, 934–942.
87. Huang, D. M.; Faller, R.; Do, K.; Moul, A. J. Coarse-Grained Computer Simulations of Polymer/Fullerene Bulk Heterojunctions for Organic Photovoltaic Applications. *J. Chem. Theory Comput.* 2010, *6*, 526–537.
88. Tapping, P. C.; Clafton, S. N.; Schwarz, K. N.; Kee, T. W.; Huang, D. M. Molecular-Level Details of Morphology-Dependent Exciton Migration in Poly(3-Hexylthiophene) Nanostructures. *J. Phys. Chem. C* 2015, *119*, 7047–7059.
89. Agrawal, V.; Arya, G.; Oswald, J. Simultaneous Iterative Boltzmann Inversion for Coarse-Graining of Polyurea. *Macromolecules* 2014, *47*, 3378–3389.
90. Lee, C.-K.; Pao, C.-W.; Chu, C.-W. Multiscale Molecular Simulations of the Nanoscale Morphologies of P3HT:PCBM Blends for Bulk Heterojunction Organic Photovoltaic Cells. *Energy Environ. Sci.* 2011, *4*, 4124–4132.
91. Do, K.; Ravva, M. K.; Wang, T.; Brédas, J.-L. Computational Methodologies for Developing Structure–Morphology–Performance Relationships in Organic Solar Cells: A Protocol Review. *Chem. Mater.* 2016, *29*, 346–354.
92. Do, K.; Risko, C.; Anthony, J. E.; Amassian, A.; Brédas, J.-L. Dynamics, Miscibility, and Morphology in Polymer-Molecule Blends: The Impact of Chemical Functionality. *Chem. Mater.* 2015, *27*, 7643–7651.
93. Carrillo, J.-M. Y.; Seibers, Z.; Kumar, R.; Matheson, M. A.; Ankner, J. F.; Goswami, M.; Bhaskaran-Nair, K.; Shelton, W. A.; Sumpter, B. G.; Kilbey, S. M. Petascale Simulations of the Morphology and the Molecular Interface of Bulk Heterojunctions. *ACS Nano* 2016, *10*, 7008–7022.
94. Alessandri, R.; Uusitalo, J. J.; de Vries, A. H.; Havenith, R. W. A.; Marrink, S. J. Bulk Heterojunction Morphologies with Atomistic Resolution from Coarse-Grain Solvent Evaporation Simulations. *J. Am. Chem. Soc.* 2017, *130*, 3697–3705.
95. Karayiannis, N. C.; Kröger, M. Combined Molecular Algorithms for the Generation, Equilibration and Topological Analysis of Entangled Polymers: Methodology and Performance. *Int. J. Mol. Sci.* 2009, *10*, 5054–5089.
96. Hoy, R. S.; Foteinopoulou, K.; Kröger, M. Topological Analysis of Polymeric Melts: Chain-Length Effects and Fast-Converging Estimators for Entanglement Length. *Phys. Rev. E* 2009, *80*, 031803.
97. Everaers, R. Rheology and Microscopic Topology of Entangled Polymeric Liquids. *Science.* 2004, *303*, 823–826.
98. Zhao, B.; Zikry, M. A. The Effects of Structural Disorders and Microstructural Mechanisms on Semi-Crystalline P3HT Behavior. *Polymer.* 2015, *57*, 1–11.
99. Dennler, G.; Scharber, M. C.; Brabec, C. J. Polymer-Fullerene Bulk-Heterojunction Solar Cells. *Adv. Mater.* 2009, *21*, 1323–1338.

100. Mayer, A. C.; Toney, M. F.; Scully, S. R.; Rivnay, J.; Brabec, C. J.; Scharber, M.; Koppe, M.; Heeney, M.; McCulloch, I.; McGehee, M. D. Bimolecular Crystals of Fullerenes in Conjugated Polymers and the Implications of Molecular Mixing for Solar Cells. *Adv. Funct. Mater.* 2009, *19*, 1173–1179.
101. Koppe, M.; Scharber, M.; Brabec, C.; Duffy, W.; Heeney, M.; McCulloch, I. Polyterthiophenes as Donors for Polymer Solar Cells. *Adv. Funct. Mater.* 2007, *17*, 1371–1376.
102. Campoy-Quiles, M.; Kanai, Y.; El-Basaty, A.; Sakai, H.; Murata, H. Ternary Mixing: A Simple Method to Tailor the Morphology of Organic Solar Cells. *Org. Electron.* 2009, *10*, 1120–1132.
103. Miller, N. C.; Cho, E.; Gysel, R.; Risko, C.; Coropceanu, V.; Miller, C. E.; Sweetnam, S.; Sellinger, A.; Heeney, M.; McCulloch, I.; Brédas, J. L.; Toney, M. F.; McGehee, M. D. Factors Governing Intercalation of Fullerenes and Other Small Molecules between the Side Chains of Semiconducting Polymers Used in Solar Cells. *Adv. Energy Mater.* 2012, *2*, 1208–1217.
104. Printz, A. D.; Savagatrup, S.; Rodriquez, D.; Lipomi, D. J. Role of Molecular Mixing on the Stiffness of Polymer:Fullerene Bulk Heterojunction Films. *Sol. Energy Mater. Sol. Cells* 2015, *134*, 64–72.
105. Anctil, A.; Babbitt, C. W.; Raffaelle, R. P.; Landi, B. J. Cumulative Energy Demand for Small Molecule and Polymer Photovoltaics. *Prog. Photovoltaics Res. Appl.* 2012, *21*, 1541–1554.
106. Savagatrup, S.; Rodriquez, D.; Printz, A. D.; Sieval, A. B.; Hummelen, J. C.; Lipomi, D. J. PCBM and Incompletely Separated Grades of Methanofullerenes Produce Bulk Heterojunctions with Increased Robustness for Ultra-Flexible and Stretchable Electronics. *Chem. Mater.* 2015, *27*, 3902–3911.
107. Awartani, O.; Lemanski, B. I.; Ro, H. W.; Richter, L. J.; De Longchamp, D. M.; O'Connor, B. T. Correlating Stiffness, Ductility, and Morphology of Polymer:Fullerene Films for Solar Cell Applications. *Adv. Energy Mater.* 2013, 3, 399–406.
108. Dupont, S. R.; Oliver, M.; Krebs, F. C.; Dauskardt, R. H. Interlayer Adhesion in Roll-to-Roll Processed Flexible Inverted Polymer Solar Cells. *Sol. Energy Mater. Sol. Cells* 2012, *97*, 171–175.